Incorporating Horizontal Density Variations into Large-scale Modelling of Ice Masses

Camilla A. O. Schelpe[1] and G. Hilmar Gudmundsson[1]

[1]Department of Geography and Environmental Sciences, Northumbria University, Newcastle upon Tyne, UK

Key Points:

- We examine the impact of horizontal variations in ice density on large-scale ice-sheet simulations.
- A commonly used approximation, which adjusts the glacial thickness to account for density variations, has a number of shortcomings.
- An approach which explicitly includes horizontal density variations could potentially lead to a 10% correction in estimated sea level rise.

Corresponding author: Camilla Schelpe, camilla.schelpe@northumbria.ac.uk

This article has been accepted for publication and undergone full peer review but has not been through the copyediting, typesetting, pagination and proofreading process, which may lead to differences between this version and the Version of Record. Please cite this article as doi: 10.1029/2022JF006744.

Abstract

Gravity-driven flow of large ice masses such as the Antarctic Ice Sheet (AIS) depends on both the geometry and the mass density of the ice sheet. The vertical density profile can be approximated as pure ice overlain by a firn layer of varying thickness, and for the AIS the firn thickness is not uncommonly 10 to 20% of the total thickness, leading to not insignificant variation in density. Nevertheless, in most vertically-integrated ice-flow models today the density is assumed constant, sometimes with an adjustment in thickness to compensate. In this study, we explore the treatment of horizontal density variations (HDVs) within vertically-integrated ice-sheet models. We assess the relative merits and shortcomings of previously proposed approaches, and provide new formulations for including HDVs. We use perturbation analysis to derive analytical solutions that describe the impact of density variations on ice flow for both grounded ice and floating ice shelves, which reveal significant qualitative differences between each of the proposed density formulations. Furthermore, by modelling the transient evolution of a large sector of the West Antarctic Ice Sheet (WAIS), we quantify the potential impact of HDVs on estimated sea level change. For the domain we considered, we find that explicitly including the horizontal density gradients in the momentum and mass conservation equations leads to about a 10% correction in the estimated change in volume above flotation over 40 years. We conclude that including horizontal density variations in flow modelling of the Antarctic Ice Sheet is important for accurate predictions of mass loss.

Plain Language Summary

Variation in the average ice-density across large ice sheets such as the Antarctic Ice Sheet will have an impact on the dynamics of the ice-flow. The question we wish to answer in this study is how significant this impact is and how best to model the density variations within large-scale numerical simulations. Variations in the average ice-sheet density come from layers of compactified snow which have a lower density than the underlying ice. Within the Antarctic Ice Sheet this compactified snow layer is approximately 10 to 20% of the total thickness, which leads to not insignificant variation in the average density. Nevertheless, in most numerical models that simulate the flow of large ice sheets, these variations are either ignored completely or approximated by an adjustment in the total ice-thickness. In all large-scale numerical models, there is a trade-off between computational complexity and an accurate depiction of the physical processes. We propose several formulations for including density variations, and study the theoretical behaviour of ice flows in each formulation. We find that numerical simulations of the Western Antarctic Ice Sheet over 40 years suggest that explicitly including density variations could potentially lead to a 10% correction in estimated sea level rise.

1 Introduction

Ice sheets typically comprise a core of meteoric ice, and an overlying layer of lower-density firn of variable thickness. This gives rise to spatial variation in the vertically-averaged density of the ice at each point on the surface. These density variations can be significant. For example, in Figure 1 we have plotted the vertically-averaged density over the ice shelves fringing the Antarctic Ice Sheet, extracted from estimates of firn thickness. We see a reduction in density of at least 5% over wide areas, and over many ice-shelves such as George IV and towards the calving fronts of the Filchner-Ronne and Ross ice shelves the reduction in average density can be as much as 15%. For unconfined ice shelves the local spreading rate is proportional to the third power of the local density (when using typical values to describe the rheology of ice), which would suggest that in some cases density variations could lead to a 40% reduction in estimated spreading rates. For grounded ice sheets the velocity is similarly impacted by the local density. Nevertheless, despite potentially having significant impact on ice flow, horizontal variations in the ice density

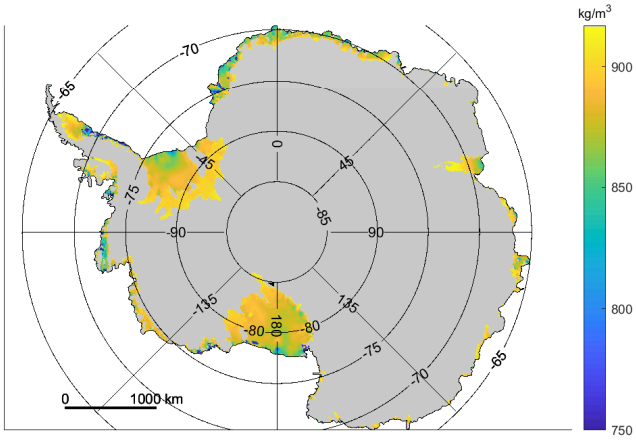

Figure 1. Vertically-averaged density of the ice-shelves in Antarctica, with the grounded domain masked (data extracted from BedMachine Antarctica (Morlighem, 2020; Morlighem et al., 2020)).

are generally not accounted for in most vertically-integrated large-scale ice sheet models today.

Here we provide the first systematic assessment of the impact of horizontal density variations on the flow of large ice masses and present new formulations for their inclusion in large-scale ice-flow models. We base our analysis on the *shallow ice stream approximation*, a commonly used vertically-integrated formulation in ice-flow modelling for describing the ice flow of large ice masses where the ice thickness is small compared to the horizontal span. (This formulation is also referred to as the shallow-shelf approximation or the shelfy approximation, and often abbreviated to SSA.) The SSA is deployed in many numerical simulation models of large ice masses. See, for example: the Pollard & DeConto Hybrid Ice Shelf Model (Pollard & DeConto, 2012), the MALI variable-resolution ice sheet model (Hoffman et al., 2018), PISM (Bueler & Brown, 2009), BISICLES (Cornford et al., 2013), f.ETISh (Pattyn, 2017), ISSM (Larour et al., 2012), and Úa (Gudmundsson, 2020b). The treatment of density variations is rarely mentioned in the literature on these ice-sheet models. In the published model descriptions, the vertically-averaged density, ρ, enters the SSA equations of mass and momentum conservation, but in all models, with the exception of Úa, the spatial and temporal derivatives of ρ appear to be set to zero. If any correction for HDVs is included, it appears to be done through modification of ice thickness. In the ice-flow model Úa, a variable density field can be specified as an input to the model, and a correction to the momentum and mass conservation equations is included. We return later to a detailed description of the implementation in Úa.

In all that follows, we consider variations in the vertically-averaged density as an input field to the ice-sheet model, similar to other input fields like the ice sheet bedrock topography or surface mass balance. We allow the density field to evolve in some of the models through advection, but we do not concern ourselves with how these variations in density arise or evolve in response to external climate forcings. The input density field can be extracted from datasets of ice and firn thicknesses, available for both the Greenland and the Antarctic Ice Sheets, e.g. the BedMachine Antarctica dataset (Morlighem, 2020; Morlighem et al., 2020). Typically, the total thickness of the ice sheet is considered to comprise an ice layer of fixed density $\rho_{\text{ice}} = 917\,\text{kg/m}^3$, and a variable firn layer for which the *firn air-content*, δ, is estimated. The firn air-content can be considered to

be the vertical distance by which the firn needs to be compacted for it to have acquired the same density as ice. From the definition of δ it follows that it can be expressed as $\delta = h \times (1 - \rho/\rho_{\text{ice}})$, where h is the total thickness of the ice column. Under this definition, $h_{\text{ice}} = h - \delta$ is the *ice-equivalent thickness*, for which $\rho_{\text{ice}} \times h_{\text{ice}} = \rho \times h$. See Appendix A for a more detailed description.

A common approach to handle density variations in ice-flow models is to adjust the height of the glacier to this *ice-equivalent thickness*, while keeping the ice-density constant $\rho = \rho_{\text{ice}}$. This preserves the total mass of the ice-column at each spatial coordinate and thus maintains hydrostatic equilibrium of the ice-shelves. We refer to this approximation as the *density-to-thickness* (D2T) adjustment method. The apparent advantage of this approach is that, as a result, all spatial density gradients in the original data sets disappear, and so no modification of the standard form to the SSA equations is required. However, this commonly used approach may not capture the true impact of density variations acting within the mass and momentum conservation equations. It is important to realize that the D2T adjustment results in modification to all terms involving ice thickness in the SSA equations, including several terms that do not involve the density. Furthermore, once the ice thickness has been modified in this manner in the initial model setup, the density variations are effectively advected with the ice over time. In what follows, we analyse the ice flow under the D2T adjustment and propose a number of alternative formulations for incorporating HDVs into large-scale ice-flow models. In particular, we examine the magnitude of the difference, or the error, when the variations in density are folded into the ice thickness distribution, as done in the D2T adjustment, compared to introducing the spatial gradients in density directly as additional terms in the SSA equations, and solving the resulting augmented system of flow equations.

We start by presenting the field equations governing ice-flow in the presence of a spatially varying density field within the SSA in section 2, with the derivation detailed in Appendix A. In section 3, we discuss various approaches for including HDVs in vertically-integrated ice-flow models, including the D2T adjustment approach outlined above. One of the first questions to consider is the general importance of horizontal density variations, and whether they can reasonably be ignored. To this end, in section 4 we start by looking at typical spatial scales governing large-scale ice flow to assess the relative size of different terms in the momentum equations, particularly those terms containing the spatial gradients in density.

The bulk of this paper is dedicated to comparing the behaviour of the different density approaches within a linearised version of the field equations. This analytical approach focuses on the response to small perturbations in the density field, closely following the approach of Gudmundsson (2008). In sections 5 and 6, we derive the transfer functions for induced perturbations in the glacial thickness and surface velocity relative to two steady-state reference solutions: that of a grounded ice sheet in section 5, and that of a floating ice shelf in section 6. The transfer functions describe the response of the primary fields to density perturbations at different spatial wavelengths. The application to a floating ice shelf is complicated by the fact that the steady-state thickness and velocity fields are spatially varying, and here we use the approximation proposed by Ng et al. (2018) for perturbation analysis in the presence of a spatially varying background field. We derive sixteen transfer functions in total: for the surface topography and horizontal velocity field within each of the four density formulations, applied to each of the two reference states. If the reader is less interested in the technical details of these derivations, they may choose to skip forward to section 7, where we summarise the derived transfer functions, although we do recommend paying attention to the details of the D2T formulation in section 5.5. In section 7 we compare the different transfer functions and use them to examine the behaviour of the ice flow in a few simple simulations.

Finally, in section 8, we look at a specific example of the impact of the different density formulations on transient simulations of the Western Antarctic ice sheet within the shallow ice-model Úa. This is applied to a limited set of the different density formulations, restricted to those that can be applied to large-scale numerical simulations within the current set of ice-flow models. We conclude in section 9 with a summary of the important findings of this study.

2 The SSA Field Equations with Horizontal Density Variations

The equations of motion describing the flow of isothermal masses are governed by the principles of conservation of mass and momentum. In this study, we restrict our analysis to ice flows that can be described by the shallow ice stream approximation (SSA), where the ice thickness is small compared to the horizontal span. The SSA equations have been derived numerous times in the literature with the first derivation being, to our knowledge, by MacAyeal (1989). Baral et al. (2001) provides a useful overview of asymptotic theories of large-scale glacier flow. In the presence of horizontal density variation, we show how the SSA mass and momentum equations need to be modified in Appendix A. We have broadly followed the derivation given in Gudmundsson (2020a), but made various modifications and extensions to account for a variable density field, resulting in several additional terms to the momentum equations. The results are summarised below. In this derivation, we make the simplifying assumption that the density is constant with depth, and equal to the vertically averaged density at each spatial point (x, y). Without this assumption, analytical solutions to the vertically-integrated field equations are not possible, and would instead require numerical integration in the z-dimension. In Appendix B we discuss this assumption and its potential short-comings in a bit more detail.

The SSA momentum-conservation equations, in the presence of a horizontally varying density field are

$$\begin{aligned}
\partial_x \left(4h\eta\partial_x u + 2h\eta\partial_y v + \frac{2h\eta}{\rho}\frac{D\rho}{Dt} \right) & \\
+\partial_y(h\eta(\partial_x v + \partial_y u)) - t_{bx} &= \rho g h \left(\partial_x s \cos\alpha - \sin\alpha\right) + \frac{1}{2}h^2 g \partial_x \rho \cos\alpha \\
\partial_y \left(4h\eta\partial_y v + 2h\eta\partial_x u + \frac{2h\eta}{\rho}\frac{D\rho}{Dt} \right) & \\
+\partial_x(h\eta(\partial_x v + \partial_y u)) - t_{by} &= \rho g h \partial_y s \cos\alpha + \frac{1}{2}h^2 g \partial_y \rho \cos\alpha \qquad (1)
\end{aligned}$$

in a tilted coordinate system aligned to the bed topography, where α is the angle of the coordinate system to the horizontal. Allowing the density field to vary has introduced two new contributions to these equations. On the left hand side, we have a term proportional to the material derivative of the density field, $D\rho/Dt$. This additional term represents momentum transfer between regions of low and high density. On the right hand side of the equations we have an additional driving term which scales as the horizontal gradient of the density. In this notation: η is the vertically-integrated effective viscosity; u, v are the horizontal velocities in the x, y directions respectively; t_{bx}, t_{by} are the horizontal components of the basal traction vector; s is the location of the upper glacial surface; and g is the acceleration due to gravity. We use the short-hand $\partial_x \equiv \frac{\partial}{\partial x}$, and the material derivative is defined as

$$\frac{D\rho}{Dt} \equiv \partial_t \rho + \boldsymbol{v} \cdot \boldsymbol{\nabla} \rho,$$

where $\boldsymbol{v} = (u, v, w)$ is the velocity vector of the ice-flow. All variables are defined throughout the text and summarised in the Notation section.

In three-dimensions, the generalised form of the mass-conservation equation which allows for density variation in the ice sheet is

$$\frac{D\rho}{Dt} + \rho \boldsymbol{\nabla} \cdot \boldsymbol{v} = 0 \tag{2}$$

In the SSA, the vertically-integrated form of this equation is

$$\rho \partial_t h + \boldsymbol{\nabla}_{xy} \cdot \boldsymbol{q}_{xy} + h \partial_t \rho = \rho a \tag{3}$$

where the horizontal mass-flux $\boldsymbol{q}_{xy} \equiv \int_b^s \rho \boldsymbol{v}_{xy} \, \mathrm{d}z$; and the total accumulation, $a = a_s + a_b$, is the sum of the surface accumulation and basal melt rates.

In addition to these field equations, the modification to the mass-conservation equation also impacts a few other expressions used inside shallow ice-flow models. Firstly, the boundary conditions at the calving front become

$$\begin{aligned} 2\eta h \left(2\partial_x u + \partial_y v + \frac{1}{\rho}\frac{D\rho}{Dt} \right) n_x + \eta h \left(\partial_x v + \partial_y u \right) n_y &= \frac{1}{2} g \left(\rho h^2 - \rho_w d^2 \right) n_x \\ 2\eta h \left(2\partial_y v + \partial_x u + \frac{1}{\rho}\frac{D\rho}{Dt} \right) n_y + \eta h \left(\partial_x v + \partial_y u \right) n_x &= \frac{1}{2} g \left(\rho h^2 - \rho_w d^2 \right) n_y \end{aligned} \tag{4}$$

where n_x and n_y are the components of the unit normal pointing horizontally outwards from the ice front; ρ_w is the density of the ocean; and the draft at the ice-front $d \equiv S - b$ where S is the surface of the ocean. Secondly, when calculating the effective viscosity in Glen's flow law, one should use

$$\dot{\epsilon}_{zz}^2 = \left(\dot{\epsilon}_{xx} + \dot{\epsilon}_{yy} + \frac{1}{\rho}\frac{D\rho}{Dt} \right)^2 \tag{5}$$

instead of $\dot{\epsilon}_{zz} = -(\dot{\epsilon}_{xx} + \dot{\epsilon}_{yy})$, where $\dot{\epsilon}_{ij}$ are the strain rates.

3 Approaches to include Horizontal Density Variations in the SSA

There are a number of approaches we could take to handle the additional terms in the modified SSA equations when modelling ice-flow. The simplest would be to ignore the density variation completely and set the material derivative and spatial gradients of the density field to zero. An alternative, which is commonly used, is to treat the density as constant and adjust the input ice-thickness by the firn air-content, as discussed in section 1. We refer to this as the **Density-to-Thickness Adjustment [D2T]** formulation. In this approximation, we set $\rho = \rho_{\text{ice}}$ and $h = h_{\text{ice}}$ in all the field equations listed in section 2. Derivative terms in ρ will implicitly be introduced by the δ adjustment to the derivative terms in h.

A more realistic formulation is implemented in the shallow-ice model Úa (Gudmundsson, 2020b), which allows a spatially-variable density field as one of the inputs. We refer to this as the **Density Variations - Body Force only [DV-BF]** formulation. Additional terms arising from the horizontal gradient of the density are included in the momentum and mass–conservation equations. It assumes a static density distribution, i.e. $\partial_t \rho = 0$. According to Sorge's law (Bader, 1954), which was based on observations of the density distribution in central Greenland, the ice density at a given depth generally does not change significantly over time. The compactification of snow into ice leads to a static density distribution, with the arrival of new low-density firn approximately balanced by the compactification and advection of existing material. However, this DV-BF formulation neglects the term in $D\rho/Dt$ on the left hand side of the momentum equation (and similarly does not modify the calving front boundary conditions nor the effective viscosity), which only leaves the correction to the body-force term on the right hand side of the momentum equation. There is a scaling argument which may justify that this is the more

significant correction term for real ice-flows, which we discuss in section 4. The correction to the mass-conservation equation is implicit in the horizontal density variation of the mass-flux.

We propose two further formulations for incorporating horizontal density variations into ice-flow models. The first is a fuller implementation of the DV-BF formulation which does not neglect the $D\rho/Dt$ terms. We refer to this as the **Density Variations [DV]** formulation. It assumes a static density distribution, thus setting $\partial_t \rho = 0$ and $D\rho/Dt = \boldsymbol{v}\cdot\boldsymbol{\nabla}\rho$ inside all the field equations in section 2. This leads to correction terms on both the left and right hand side of the momentum equations. However, this formulation does cause some conceptual difficulties as the left hand side of the momentum equation is no longer frame-invariant, which is inevitable since in order to assume $\partial_t \rho \approx 0$ we must be specifying a particular reference frame.

This lack of frame-invariance motivates our second proposal, which is to allow the temporal evolution of the vertically-integrated density field. We refer to this as the **Density Variations Advected [DVA]** formulation. We ignore the overhead snow accumulation and compactification at depth, and assume that the initial density distribution advects with the ice, such that the flow is density-preserving. In this limit we set $D\rho/Dt = 0$ in all the field equations listed in section 2, and the density evolves according to $\partial_t \rho = -\boldsymbol{v}\cdot\boldsymbol{\nabla}\rho$. The DVA formulation is not a particularly realistic scenario, since it is the overhead snow accumulation and compacitifaction which gives rise to the HDVs in the first place. However, we find the behaviour in the DVA formulation a helpful comparison for some of the behaviour observed in the D2T formulation, and it represents the opposing limit to the case of a static density distribution in the DV formulation. A full treatment that includes a detailed firn compactification model to estimate the evolution of the vertically-integrated density at each spatial coordinate is best kept to an external atmospheric model that updates a static density distribution over time. We discuss this further in the conclusions.

We consider each of these four approaches for including horizontal density variations (DV, DV-BF, DVA and D2T) independently in the perturbation analysis that follows in sections 5 and 6, and compare the results of the different approaches in 7. In the numerical simulations of the Antarctic Ice Sheet in section 8, we are obliged to restrict our analysis to comparing the DV-BF and D2T adjustment methods, which are the only two formulations that are enabled for large-scale simulations in current ice-flow models.

4 Significance of the Additional Density Variation Terms

One of the first questions to consider is the relative magnitude of the additional terms in the SSA equations that arise in the presence of a varying density field, as derived in section 2, regardless of the specific density formulation used.

We start with the modified momentum-conservation equation, and look at the typical scales for the different variables, indicated by $[\cdot]$. Restricted to one-dimensional flow, and assuming that time scales advectively, i.e. $D\rho/Dt$ scales as $\boldsymbol{v}\cdot\boldsymbol{\nabla}\rho$, Equation (1) can be expressed in terms of the typical scales as

$$\frac{4[\eta][h][u]}{[x]^2}\left(\frac{[\Delta u]}{[u]}+\frac{1}{2}\frac{[\Delta\rho]}{[\rho]}\right)-[t_{bx}]=\frac{[\rho][g][h]^2}{[x]}\left(\frac{[\Delta s]}{[h]}+\frac{1}{2}\frac{[\Delta\rho]}{[\rho]}\right)-[\rho][g][h][\alpha]$$

where $[\alpha] = [h]/[x] \ll 1$ in the shallow ice stream approximation. The scale $[\Delta\rho]$ represents the variation in density over the horizontal length scale $[x]$. The additional terms on both the right and left hand sides of the momentum equation scale as $[\Delta\rho]/[\rho]$. The same is true of the additional terms in the D2T adjustment method, which scale as $[\delta]/[h] = [\Delta\rho]/[\rho]$. A reasonable estimate from Figure 1 is that the average density of an ice sheet can range from $917\,\mathrm{kg\,m^{-3}}$ to approximately $830\,\mathrm{kg\,m^{-3}}$, such that $[\Delta\rho]/[\rho] \sim 0.1$. Standard scaling arguments would argue that $[\Delta u]/[u] \sim 1$ and $[\Delta s]/[h] \sim 1$, which would

imply that the density terms on both sides of the momentum equation contribute equally, with a magnitude of approximately 10%.

The true relative contribution of the additional density terms will depend on the glacier topography. For example with grounded ice caps, which typically exhibit larger variations in $[\Delta s]$, the basal drag t_{bx} tends to dominate on the left hand side of the momentum equation. Under this scenario, we might expect the density correction term on the left hand side to be negligible, and only the correction to the body-force term to be significant. For fast flowing ice streams and floating ice-shelves, the basal drag tends to zero. However the surface slope, $[\Delta s]$, also tends to zero, at which point the density correction in the body-force term may become quite significant. In both scenarios, this is suggestive that the density correction term within the driving force on the right hand side of the momentum equation is more significant than that on the left, and should be prioritised in the implementation of any horizontal density formulation. This is consistent with the DV-BF formulation which prioritises the body-force term, as opposed to the more complete DV formulation which includes both terms.

The additional density terms in both the mass-conservation equation and the calving front boundary conditions, in Equations (3) and (4), can also be seen to contribute approximately 10%. The contribution to the effective viscosity from Equation (5) is less obvious. It can be shown that it ultimately introduces a multiplicative factor to the effective viscosity, which scales as $\left(1 - \frac{n-1}{2n}\frac{[\Delta\rho]}{[\rho]}\right)$. Typical values for the exponent in Glen's flow law, $n = 3$, would suggest that this correction is less significant, but not negligible, at 3%.

5 Perturbation Analysis: The Case of a Grounded Ice-Sheet

We wish to understand the impact on the ice flow of including the additional terms arising from horizontal density variations. In this section and the next (section 6) we derive the transfer functions describing the first-order response to small perturbations in the glacial density. We follow closely the technique presented in Gudmundsson (2008), and derive transfer functions for the induced perturbations in the surface $s(x,t)$ and horizontal velocity $u(x,t)$, restricted to the one-dimensional case for simplicity. In this section we focus on the reference state of a grounded ice sheet, and derive the response to small perturbations about this reference solution. We do this separately for each of the four density formulations (DV, DV-BF, DVA, D2T) that were described in section 3. If the reader is less interested in the mathematical details of these derivations, they can skip forward to section 7 which summarises and analyses the different transfer functions, although we do recommend paying attention to the derivation in the D2T formulation in section 5.5.

We start by describing the reference solution for the grounded ice-sheet in section 5.1. In section 5.2 we go through the steps to derive the transfer functions in the DV formulation in detail. This illustrates the technique, and then for each subsequent derivation (in sections 5.3 to 5.5) we only include steps which require a different treatment. In outline, the steps in each derivation are to take the relevant momentum and mass conservation equations, together with the kinematic boundary conditions, to arrive at a system of differential equations which relate small perturbations in the density and surface fields. Taking the Fourier and Laplace transforms turns this into a linearised system of equations, which can be solved to arrive at the transfer functions. These describe the phase and amplitude of surface field perturbations in response to a prescribed density perturbation as a function of frequency and time.

5.1 Reference Solution

In the case of a grounded ice sheet, the basal stress can be described by Weertman's sliding law:

$$t_{bx} = c^{-1/m} \|\boldsymbol{v_b}\|^{1/m-1} \boldsymbol{v_b}$$

where $\boldsymbol{v_b}$ is the basal velocity and c is the slipperiness along the bed. In the SSA, the horizontal velocities are constant with depth and so in one-dimension $t_{bx} = (u/c)^{1/m}$. In this perturbation analysis, we assume that the viscosity is linear such that $\eta = \text{const}$. Taking the vertically-integrated SSA momentum equations presented in Equation (1), and restricting to a one-dimensional flow-line for simplicity, we find

$$\partial_x \left(4h\eta \partial_x u + \frac{2h\eta}{\rho} \frac{D\rho}{Dt} \right) - \left(\frac{u}{c} \right)^{1/m} = \rho g h \left(\partial_x s \cos\alpha - \sin\alpha \right) + \frac{1}{2} g h^2 \partial_x \rho \cos\alpha \qquad (6)$$

We consider an idealised scenario of flow down a uniformly inclined slab of constant thickness, which extends infinitely in the x and y dimensions. To find the steady-state reference solution, we look for solutions which are independent of x. This can be solved trivially to find

$$u = c(\rho g h \sin\alpha)^m$$

which is our reference solution for the flow.

5.2 Perturbations within the DV formulation

Our first example is to apply a small density perturbation to the ice sheet, and assume the ice dynamics can be described by a static density distribution as specified by the *Density Variations* [DV] formulation.

Within this perturbation analysis, we apply a small perturbation to the ice density about a constant reference value:

$$\rho(x,t) = \bar{\rho} + \Delta\rho(x,t) \qquad (7)$$

while holding other parameters constant, such as the viscosity η and basal slipperiness c. This induces small perturbations in the other variables:

$$\begin{aligned} h(x,t) &= \bar{h}(x) + \Delta h(x,t) \\ s(x,t) &= \bar{s}(x) + \Delta s(x,t) \\ u(x,t) &= \bar{u}(x) + \Delta u(x,t) \\ w(x,z,t) &= \bar{w}(x,z) + \Delta w(x,z,t) \end{aligned} \qquad (8)$$

In the case of a grounded ice sheet, the reference solution is independent of x and so $\bar{u}$, $\bar{h}$ and $\bar{s}$ are constants, while $\bar{w}$ is a function of z only. The lower surface remains unperturbed, such that $\bar{h} = \bar{s} - \bar{b}$ and $\Delta s = \Delta h$. In the DV formulation, the density distribution is held static, so we assume the perturbation in time is a step function $\mathcal{H}(t)$ with zero perturbation before $t = 0$, and a fixed contribution which varies with x thereafter: $\Delta\rho(x,t) = \mathcal{H}(t)\Delta\rho(x)$.

In the DV formulation, the momentum and mass conservation equations describing the ice flow, Equations (6) and (2) respectively, become

$$\begin{aligned} \partial_x \left(4h\eta \partial_x u + \frac{2h\eta}{\rho} u \partial_x \rho \right) - \left(\frac{u}{c} \right)^{1/m} &= \rho g h \left(\partial_x s \cos\alpha - \sin\alpha \right) + \frac{1}{2} h^2 g \partial_x \rho \cos\alpha \\ u\partial_x \rho + \rho(\partial_x u + \partial_z w) &= 0 \end{aligned}$$

Applying the perturbations of Equations (7) and (8), the momentum equation to zeroth-order is identically equal to the reference solution:

$$\bar{u} = c \left(\bar{\rho} g \bar{h} \sin\alpha \right)^m \qquad (9)$$

while to first-order in the perturbations, the equations of motion are

$$\begin{aligned} 4\bar{h}\eta\partial^2_{xx}\Delta u + \frac{2\eta\bar{h}\bar{u}}{\bar{\rho}}\mathcal{H}(t)\partial^2_{xx}\Delta\rho - \gamma\Delta u &= \tau_d\partial_x\Delta s\cot\alpha - \frac{\tau_d}{\bar{h}}\Delta s \\ &\quad -\tau_d\mathcal{H}(t)\frac{\Delta\rho}{\bar{\rho}} + \frac{1}{2}\tau_d\bar{h}\mathcal{H}(t)\frac{\partial_x\Delta\rho}{\bar{\rho}}\cot\alpha \\ \bar{u}\mathcal{H}(t)\partial_x\Delta\rho + \bar{\rho}(\partial_x\Delta u + \partial_z\Delta w) &= 0 \end{aligned} \tag{10}$$

where we have defined

$$\begin{aligned} \tau_d &\equiv \bar{\rho}g\bar{h}\sin\alpha \\ \gamma &\equiv \left(\frac{\bar{u}}{c}\right)^{1/m}\frac{1}{m\bar{u}} = \tau_d^{1-m}\frac{1}{mc} \end{aligned}$$

and the final equality comes from the zeroth-order solution.

In addition to the equations of motion, we require the kinematic boundary conditions to find analytical solutions to these perturbations. At the upper and lower surfaces respectively,

$$\begin{aligned} \partial_t s + u\partial_x s - w|_s &= a_s \\ \partial_t b + u\partial_x b - w|_b &= -a_b \end{aligned} \tag{11}$$

where all variables apart from the vertical velocity w are independent of z in the SSA. We set the accumulation rates $a_s = a_b = 0$ in the case of a grounded ice sheet, so that the reference solution is time-invariant. We need to be careful when considering the perturbation response within the boundary conditions, to separate out the perturbation in a function due to variation with the location of the boundary surface Δs, and the perturbation in the function due to other factors. Consider a function $f = f(z, \phi)$, which varies with depth, z, as well as other factors which we have aggregated together as ϕ. Using a Taylor expansion to first order,

$$\begin{aligned} f(z,\phi) &= f(\bar{z},\bar{\phi}) + \partial_z f(\bar{z},\bar{\phi})\Delta z + \partial_\phi f(\bar{z},\bar{\phi})\Delta\phi \\ &= \bar{f}(\bar{z}) + \partial_z\bar{f}(\bar{z})\Delta z + \Delta f(\bar{z}) \end{aligned}$$

where for the sake of brevity, variation due to the other factors ϕ has been aggregated into Δf. We apply this technique to the horizontal (u) and vertical (w) velocities at the boundary. We find that to zeroth order,

$$\bar{w}|_{\bar{s}} = \bar{w}|_{\bar{b}} = 0$$

while to first order,

$$\begin{aligned} \partial_t\Delta s + \bar{u}|_{\bar{s}}\partial_x\Delta s - \Delta w|_{\bar{s}} &= 0 \\ \Delta w|_{\bar{b}} &= 0 \end{aligned} \tag{12}$$

where the term in $\partial_z\bar{w}|_{\bar{s}}$ has vanished due to the zeroth-order solution.

To solve this system of first-order equations, we apply Fourier and Laplace transforms in the x and t dimensions respectively, defined as

$$\begin{aligned} f(k) &= \int_{-\infty}^{+\infty} f(x)e^{\mathrm{i}kx}\mathrm{d}x \\ f(r) &= \int_{0^+}^{+\infty} f(t)e^{-rt}\mathrm{d}t \end{aligned} \tag{13}$$

where a dependence on the spatial coordinate x is transformed into a dependence on the wavenumber $k = 2\pi/\lambda$ in the Fourier domain, and the time coordinate is transformed

into a dependence on the complex parameter r in the Laplace domain. We apply the transforms to the perturbations: $\Delta\rho$, Δs, Δu and Δw. These perturbations are functions of (x,t). In the *F.T.* and *L.T.* space they become functions of (k,r). Under these transforms, we have the following identities:

$$\begin{aligned} F.T.\left(f'(x)\right) &= -ikF.T.\left(f(x)\right) \\ F.T.\left(f''(x)\right) &= -k^2F.T.\left(f(x)\right) \\ L.T.\left(f'(t)\right) &= rL.T.\left(f(t)\right) - f(t=0^-) \\ L.T.\left(\mathcal{H}(t)\right) &= r^{-1} \end{aligned}$$

The Fourier and Laplace transforms of the first-order equations of motion and boundary conditions in Equations (10) and (12) give rise to the following linearised system of equations:

$$\xi\Delta u = ik\tau_d\Delta s\cot\alpha + \frac{\tau_d}{\bar{h}}\Delta s + \left(\tau_d + ik\frac{\tau_d\bar{h}}{2}\cot\alpha - 2\eta\bar{h}\bar{u}k^2\right)\frac{\Delta\rho}{\bar{\rho}r} \tag{14}$$

$$\partial_z\Delta w = ik\Delta u + ik\bar{u}r^{-1}\Delta\rho/\bar{\rho} \tag{15}$$

$$\Delta w|_{\bar{s}} = r\Delta s - ik\bar{u}\Delta s \tag{16}$$

$$\Delta w|_{\bar{b}} = 0 \tag{17}$$

where we have defined

$$\xi \equiv \gamma + 4\bar{h}k^2\eta$$

and we have chosen to set $\Delta s(t=0^-)=0$. In the SSA equations, only Δw is a function of z, and so we can integrate Equation (15) between the lower and upper surfaces and apply the boundary conditions given by Equations (16) and (17), to give

$$(r - ik\bar{u})\Delta s = ik\bar{h}\Delta u + ik\bar{h}\bar{u}r^{-1}\Delta\rho/\bar{\rho}$$

We eliminate Δu by inserting Equation (14), and collect terms in $\Delta\rho$ and Δs to arrive at the transfer function

$$T_{s\rho}(k,r) \equiv \frac{\Delta s(k,r)}{\Delta\rho(k)} = \frac{\bar{h}\left(p + \frac{1}{2}t_r^{-1} - ik\bar{u}\zeta\right)}{\bar{\rho}r\left(r-p\right)}$$

where, following the definitions in Gudmundsson (2008), we have defined

$$\begin{aligned} p &\equiv it_p^{-1} - t_r^{-1} \\ t_p^{-1} &\equiv k\left(\bar{u} + \tau_d\xi^{-1}\right) \\ t_r^{-1} &\equiv \xi^{-1}k^2\tau_d\bar{h}\cot\alpha \end{aligned}$$

in addition to

$$\zeta \equiv 2\eta\bar{h}k^2\xi^{-1}\,.$$

We convert $T_{s\rho}(k,r)$ back into the time dimension through the inverse Laplace transform:

$$f(t) = \frac{1}{2\pi i}\int_{\gamma-i\infty}^{\gamma+i\infty} e^{rt}f(r)\mathrm{d}r$$

Note in this context γ is an arbitrary real number so that the contour path of integration is in the region of convergence of $f(r)$, not to be confused with the earlier parameter γ in the field equations. The function $T_{s\rho}(k,r)$ has two poles: one at $r=0$ and one at $r=p$. The quantities in the definition of t_r are always positive, and so the pole defined by $r=p$ will reside in the left half of the complex plane. We integrate over the left half of the complex plane, enclosing both poles, such that the contour integral is equal to $2\pi i$ times the sum of the residuals. The function $T_{s\rho}(k,r)\to 0$ as $|r|\to\infty$, and so

by Jordan's Lemma we can ignore the arc segment of the contour integral that expands to infinity. Thus,

$$T_{s\rho}(k,t) \equiv \frac{\Delta s(k,t)}{\Delta\rho(k)} = \frac{\bar{h}\left(p + \frac{1}{2}t_r^{-1} - ik\bar{u}\zeta\right)}{\bar{\rho}p}\left(e^{pt} - 1\right) \tag{18}$$

This transfer function has two components: an exponential term e^{pt} which decays over time (since p resides in the left half of the complex plane), and a steady-state component which means a perturbation will persist in the glacial surface. Numerical integration is required to transform the response in the surface from the frequency domain into the spatial domain, with the inverse Fourier transform:

$$\Delta s(x,t) = \int_{-\infty}^{\infty} T_{s\rho}(k,t)\Delta\rho(k)e^{-ikx}\mathrm{d}k \tag{19}$$

where $\Delta\rho(k)$ is the Fourier transform of the small perturbation in the density field $\Delta\rho(x)$.

We can follow a similar procedure to find the response of the horizontal velocity to perturbations in the density. In the Laplace domain,

$$\Delta u(k,r) = \left(\frac{(r - ik\bar{u})\left(\frac{1}{2}t_r^{-1} - ik\bar{u}\zeta\right) + r(p - ik\bar{u})}{r(r-p)}\right)\frac{\Delta\rho(k)}{ik\bar{\rho}}$$

and taking the inverse Laplace transform, the transfer function for the horizontal velocity in the time-domain is

$$T_{u\rho}(k,t) \equiv \frac{\Delta u(k,t)}{\Delta\rho(k)} = \frac{\bar{u}\left(\frac{1}{2}t_r^{-1} - ik\bar{u}\zeta\right)}{\bar{\rho}p} + \frac{(p - ik\bar{u})\left(p + \frac{1}{2}t_r^{-1} - ik\bar{u}\zeta\right)}{ik\bar{\rho}p}e^{pt} \tag{20}$$

5.3 Perturbations within the DV-BF formulation

We can follow exactly the same procedure to find the transfer functions when the ice-flow is described by the *Density Variations - Body Force only* [DV-BF] formulation, which just requires us to neglect the term in $u\partial_x\rho$ on the left hand side of the momentum equation. In the DV-BF formulation, the momentum and mass conservation equations describing the ice flow, Equations (6) and (2) respectively, become

$$\begin{aligned} \partial_x\left(4h\eta\partial_x u\right) - \left(\frac{u}{c}\right)^{1/m} &= \rho g h\left(\partial_x s\cos\alpha - \sin\alpha\right) + \frac{1}{2}h^2 g\partial_x\rho\cos\alpha \\ u\partial_x\rho + \rho(\partial_x u + \partial_z w) &= 0 \end{aligned}$$

and the derived transfer functions are

$$T_{s\rho}(k,t) \equiv \frac{\Delta s(k,t)}{\Delta\rho(k)} = \frac{\bar{h}\left(p + \frac{1}{2}t_r^{-1}\right)}{\bar{\rho}p}\left(e^{pt} - 1\right) \tag{21}$$

$$T_{u\rho}(k,t) \equiv \frac{\Delta u(k,t)}{\Delta\rho(k)} = \frac{\bar{u}\left(\frac{1}{2}t_r^{-1}\right)}{\bar{\rho}p} + \frac{(p - ik\bar{u})\left(p + \frac{1}{2}t_r^{-1}\right)}{ik\bar{\rho}p}e^{pt} \tag{22}$$

5.4 Perturbations within the DVA formulation

In this next example, we assume the ice dynamics can be described by an initial density distribution which then advects over time as specified by the *Density Variations Advected* [DVA] formulation. We follow a similar procedure to that detailed in section 5.2.

In the DVA formulation, the momentum and mass conservation equations describing the ice flow, Equations (6) and (2) respectively, become

$$\begin{aligned} \partial_x\left(4h\eta\partial_x u\right) - \left(\frac{u}{c}\right)^{1/m} &= \rho g h\left(\partial_x s\cos\alpha - \sin\alpha\right) + \frac{1}{2}h^2 g\partial_x\rho\cos\alpha \\ \partial_x u + \partial_z w &= 0 \end{aligned}$$

together with the equation of motion for the density evolution,

$$\frac{D\rho}{Dt} \equiv \partial_t \rho + u\partial_x \rho = 0 \tag{23}$$

while the kinematic boundary conditions are the same as before in Equation (12).

We apply a perturbation to the density field which can evolve over time, as described in Equations (7) and (8), with $\Delta\rho(x, t < 0) = 0$. Keeping terms to first-order in the perturbations, and applying the Fourier and Laplace transforms defined in Equation (13), we arrive at the following linearised system of equations:

$$\begin{aligned}
\xi\Delta u &= ik\tau_d \Delta s \cot\alpha + \frac{\tau_d}{\bar{h}}\Delta s + \left(\tau_d + ik\frac{\tau_d \bar{h}}{2}\cot\alpha\right)\frac{\Delta\rho}{\bar{\rho}} \\
\partial_z \Delta w &= ik\Delta u \\
r\Delta\rho - \Delta\rho_0(k) &= ik\bar{u}\Delta\rho \\
\Delta w|_{\bar{s}} &= r\Delta s - ik\bar{u}\Delta s \\
\Delta w|_{\bar{b}} &= 0
\end{aligned}$$

where the initial density distribution $\Delta\rho_0(k) \equiv \Delta\rho(k, t = 0)$, and as before we have chosen to set $\Delta s(t \leq 0) = 0$. This system of equations can be solved to arrive at

$$\Delta s(k, r) = \frac{\bar{h}\left(p - ik\bar{u} + \frac{1}{2}t_r^{-1}\right)}{(r-p)(r-ik\bar{u})\bar{\rho}}\Delta\rho_0(k)$$

which describes the surface perturbation relative to the *initial* density distribution. The poles of the transfer function are at $r = p$ and $r = ik\bar{u}$. The latter is associated with the timescale for the advection of the density distribution. Applying the inverse Laplace transform, the transfer function in frequency space is

$$T_{s\rho_0}(k, t) \equiv \frac{\Delta s(k, t)}{\Delta\rho_0(k)} = \frac{\bar{h}\left(p - ik\bar{u} + \frac{1}{2}t_r^{-1}\right)}{\bar{\rho}(p - ik\bar{u})}\left(e^{pt} - e^{ik\bar{u}t}\right) \tag{24}$$

We can follow a similar procedure to find the response of the horizontal velocity to perturbations in the density:

$$T_{u\rho_0}(k, t) \equiv \frac{\Delta u(k, t)}{\Delta\rho_0(k)} = \frac{p - ik\bar{u} + \frac{1}{2}t_r^{-1}}{ik\bar{\rho}}e^{pt} \tag{25}$$

Note that in the DVA formulation, the spatial distribution of the density at any point in time can be found by taking the inverse *F.T.* of the transfer function which relates the density to the initial density distribution:

$$T_{\rho\rho_0}(k, t) = \frac{\Delta\rho(k, t)}{\Delta\rho_0(k)} = e^{ik\bar{u}t}$$

5.5 Perturbations within the D2T formulation

Finally, we again repeat the perturbation analysis outlined in section 5.2, but this time we assume the ice flow can be described by the *Density-to-Thickness Adjustment* [D2T] formulation. The equations of motion and the boundary conditions are shifted to mimic the thickness adjustment performed in the D2T formulation, such that all variables relate to the same physical quantities.

In the D2T formulation, the density is set as a constant ρ_{ice} everywhere, and the surface of the glacier is shifted by the firn air-content, such that the height is equal to the ice-equivalent thickness: $h_{\text{ice}} \equiv h - \delta$. In this formulation, the momentum-conservation described by Equation (6) becomes

$$\partial_x\left(4(h-\delta)\eta\partial_x u\right) - t_{bx} = \rho_{\text{ice}} g(h-\delta)\left(\partial_x(s-\delta)\cos\alpha - \sin\alpha\right)$$

which can be expressed as

$$\partial_x\left(4\frac{\rho}{\rho_{\text{ice}}}h\eta\partial_x u\right)-\left(\frac{u}{c}\right)^{1/m} = \frac{\rho}{\rho_{\text{ice}}}\rho g h\partial_x s\cos\alpha-\rho g h\sin\alpha+\frac{\rho}{\rho_{\text{ice}}}g h^2\partial_x\rho\cos\alpha \tag{26}$$

where the firn air-content has been replaced by the vertically-averaged density $\rho=\rho_{\text{ice}}(1-\delta/h)$. Comparing this to Equation (6), which is the complete form of the SSA momentum equation in the presence of a varying density field, we see that, while there is some similarity in the additional terms, there are many differences which do not disappear to order $\mathcal{O}(\delta)$ in the limit $\delta \ll h$. The density is constant in the D2T formulation, and so the mass-conservation in Equation (2) becomes

$$\partial_x u+\partial_z w=0 \tag{27}$$

The kinematic boundary conditions in Equation (11) are also modified in the D2T formulation, since the location of the surface in the model is shifted. At the upper and lower surfaces respectively,

$$\begin{aligned}\partial_t(s-\delta)+u\partial_x(s-\delta)-w|_{s-\delta} &= a_s\\ \partial_t b+u\partial_x b-w|_b &= -a_b\end{aligned}$$

Combining the two boundary conditions and replacing the firn air-content with the vertically-averaged density, we find

$$\partial_t\left(\frac{\rho}{\rho_{\text{ice}}}h\right)+u\partial_x\left(\frac{\rho}{\rho_{\text{ice}}}h\right)-\left(w|_{s-\delta}-w|_b\right)=a \tag{28}$$

The firn air-content is applied as an initial static adjustment to the glacial surface in the D2T formulation, and so the applied density perturbation in this analysis is also static: $\Delta\rho(x,t) = \mathcal{H}(t)\Delta\rho(x)$. Applying the perturbations in Equations (7) and (8), the momentum equation to zeroth-order solution is identically equal to the reference solution in Equation (9), in other words the average density can equally well be expressed as a shift in the glacial thickness. This is not the case at higher orders. Keeping terms to first-order in the perturbations, and applying the Fourier and Laplace transforms defined in Equation (13), the equations of momentum and mass conservation together with the kinematic boundary conditions, become

$$\begin{aligned}\tilde{\xi}\Delta u &= \left(\frac{ik\tau_d}{\rho_{\text{ice}}}\cot\alpha+\frac{\tau_d}{\bar{\rho}\bar{h}}\right)\left(\bar{\rho}\Delta s+r^{-1}\bar{h}\Delta\rho\right)\\ \partial_z\Delta w &= ik\Delta u\\ \Delta w|_{\bar{s}-\bar{\delta}}-\Delta w|_{\bar{b}} &= (r-ik\bar{u})\frac{\bar{\rho}}{\rho_{\text{ice}}}\Delta s-ik\bar{u}r^{-1}\frac{\bar{h}}{\rho_{\text{ice}}}\Delta\rho\end{aligned}$$

where $\tau_d\equiv\bar{\rho}g\bar{h}\sin\alpha$ as before, but we have defined

$$\tilde{\xi}\equiv 4\eta\frac{\bar{\rho}}{\rho_{\text{ice}}}\bar{h}k^2+\gamma$$

There is a subtlety that is important to think about carefully when applying the Laplace transform to the kinematic boundary condition. Within the D2T adjustment, density perturbations are applied within the ice sheet geometry *before the run starts*. Therefore $\Delta\rho(x,t=0^-)=\Delta\rho(x)$. This could also be expressed as $\mathcal{H}(t=0^-)=1$ in our notation, although it diverges from the strict definition of the Heaviside step function. Both here and in the earlier analysis, we choose $\Delta s(t=0^-)=0$, i.e. we don't apply an instantaneous response in the *unmodified* glacial surface. Therefore when taking the $L.T.$ of the first term in Equation (28) to first order in the perturbations, we have

$$\begin{aligned}L.T.\left(\partial_t\left(\frac{\bar{\rho}}{\rho_{\text{ice}}}\Delta h+\frac{\bar{h}}{\rho_{\text{ice}}}\mathcal{H}(t)\Delta\rho\right)\right) &= r\left(\frac{\bar{\rho}}{\rho_{\text{ice}}}\Delta h+\frac{\bar{h}}{\rho_{\text{ice}}}r^{-1}\Delta\rho\right)-\left[\frac{\bar{\rho}}{\rho_{\text{ice}}}\Delta h+\frac{\bar{h}}{\rho_{\text{ice}}}\mathcal{H}(t)\Delta\rho\right]_{t=0^-}\\ &= \frac{\bar{\rho}}{\rho_{\text{ice}}}r\Delta h\end{aligned}$$

This system of equations can be solved to arrive at

$$T_{s\rho}(k,r) \equiv \frac{\Delta s(k,r)}{\Delta\rho(k)} = \frac{\bar{h}\tilde{p}}{\bar{\rho}r\,(r-\tilde{p})}$$

where we have defined

$$\begin{aligned}\tilde{p} &\equiv i\tilde{t}_p^{-1} - \tilde{t}_r^{-1}\\ \tilde{t}_p^{-1} &\equiv k\left(\bar{u} + \tau_d\tilde{\xi}^{-1}\right)\\ \tilde{t}_r^{-1} &\equiv \frac{\bar{\rho}}{\rho_{\text{ice}}}\tilde{\xi}^{-1}k^2\tau_d\bar{h}\cot\alpha\end{aligned}$$

Taking the inverse Laplace, the transfer function in frequency space is

$$T_{s\rho}(k,t) \equiv \frac{\Delta s(k,t)}{\Delta\rho(k)} = \frac{-\bar{h}}{\bar{\rho}}\left(1 - e^{\tilde{p}t}\right) \tag{29}$$

We observe that the time scale of this transfer function is different to those derived previously in Equations (18, 21 & 24). This is because of the dependence in the definition of δ on h, which is one of the response variables in the perturbation analysis. The location of the pole in the complex plane changes whenever the contribution to Δs changes, and with it the expression for the time scale.

We can transform this transfer function into the response observed in the adjusted surface $s_{\text{ice}} \equiv s - \delta$, using the relationship $\Delta\rho = -\rho_{\text{ice}}\Delta(\delta/h)$:

$$\frac{\Delta s_{\text{ice}}}{\Delta\rho} = \frac{\Delta(h-\delta)}{\Delta\rho} = \frac{\bar{h}}{\rho_{\text{ice}}} + \left(1 - \frac{\bar{\delta}}{\bar{h}}\right)\frac{\Delta h}{\Delta\rho} = \frac{\bar{h}}{\rho_{\text{ice}}}e^{\tilde{p}t}$$

The perturbation in the adjusted surface is equal to the firn air-content perturbation initially, and as the response evolves $\Delta s_{\text{ice}} \to 0$, such that the induced perturbation in the glacial surface decays away. If we express the perturbation in terms of the firn air-content which has units 'distance', and set $\bar{\delta} = 0$, such that $\Delta\rho = -(\rho_{\text{ice}}/\bar{h}) \times \Delta\delta$, then we find

$$\frac{\Delta s_{\text{ice}}}{\Delta\delta} = -e^{\tilde{p}t}$$

which is identical to the transfer function $-T_{ss_0}$ derived in Equation (27) of Gudmundsson (2008). This makes sense since the density perturbation expressed as $\Delta\delta$ in the D2T adjustment is identical to a shift in $s_0 = -\delta$. While over time the perturbation in the *ice-equivalent surface* dissipates, by definition this means that the unmodified surface develops a depression equal to the firn air-content of the density perturbation, giving rise to a constant transfer function at all frequencies in the steady-state.

We can follow a similar procedure to find the response of the horizontal velocity to perturbations in the density:

$$T_{u\rho}(k,t) \equiv \frac{\Delta u(k,t)}{\Delta\rho(k)} = \frac{\tilde{p} - ik\bar{u}}{ik\bar{\rho}}e^{\tilde{p}t} \tag{30}$$

Note that again this expression reduces to the transfer function T_{us_0} derived in Equation (29) of Gudmundsson (2008), if we set $\bar{\delta} = 0$ and write the perturbation in terms of the firn air-content: $T_{u\delta} = -\frac{\rho_{\text{ice}}}{\bar{h}} \times T_{u\rho}$; while at the same time restricting Equation (29) of Gudmundsson (2008) to the flow-line case by setting the transverse wave number l to zero.

6 Perturbation Analysis: The Case of a Floating Ice-Shelf

In this section, we repeat the perturbation analysis detailed extensively in section 5 for each of the four density formulations in the case of a grounded ice sheet, but this

time applied to a floating ice shelf reference state. There are a number of key differences to that of a uniform grounded ice sheet, which we highlight as we go through the derivations below. If the reader is less interested in the mathematical details of these derivations, they can skip forward to section 7 which summarises and analyses the different transfer functions.

We follow the same layout as before by describing the reference solution for the floating ice-shelf in section 6.1, and then in section 5.2 we go through the steps that are particular to deriving the transfer functions in the case of a floating ice-shelf in the DV formulation. Subsequent derivations (in sections 6.3 to 6.5) build on this derivation and only explicitly present steps which require a different treatment. In outline, the steps in each derivation are to take the relevant momentum and mass conservation equations, together with the kinematic boundary conditions, to arrive at a system of differential equations which relate small perturbations in the density and surface fields. By assuming a separation of scales, derivatives in the background thickness and velocity fields are treated as locally constant. This makes it possible to take the Fourier and Laplace transforms and arrive at a linearised system of equations. These can be solved to arrive at the transfer functions, which describe the phase and amplitude of surface field perturbations in response to a prescribed density perturbation as a function of frequency and time. The transfer functions are now additionally a function of the spatial coordinate x, due to their dependence on the value of the background field derivatives at the point of the perturbation.

6.1 Reference Solution

The equilibrium profile of a floating ice shelf is a well-known solution in glaciology, with one of the earliest derivations, to our knowledge, being that in Van der Veen (1983). We repeat the derivation in Appendix C for reference. The SSA momentum equation given by Equation (1), for a floating ice shelf restricted to a one-dimensional flow-line for simplicity, in the presence of a varying density field, is

$$\partial_x \left(4h\eta\partial_x u + \frac{2h\eta}{\rho}\frac{D\rho}{Dt} \right) = \rho g h \partial_x s + \frac{1}{2}h^2 g \partial_x \rho$$

For a floating ice shelf, the glacial height and surface are no longer offset by a constant. Instead they obey the flotation condition, where the upthrust of the ocean on the bed is equal to the weight of the water displaced, and this balances the weight of the overlying ice sheet, such that

$$s - S = h\left(1 - \frac{\rho}{\rho_w}\right) \tag{31}$$

The ocean surface is always unperturbed, $\partial_x S = 0$, and so we can substitute the relationship,

$$\partial_x s = \partial_x \left(h\left(1 - \frac{\rho}{\rho_w}\right)\right)$$

into the momentum equation, to arrive at

$$\partial_x \left(4h\eta\partial_x u + \frac{2h\eta}{\rho}\frac{D\rho}{Dt} \right) = \partial_x \left(\frac{1}{2}\rho g h^2 \left(1 - \frac{\rho}{\rho_w}\right)\right)$$

Integrating both sides, we find that momentum-conservation for a floating ice shelf with variable density, obeys

$$4\eta\partial_x u + \frac{2\eta}{\rho}\frac{D\rho}{Dt} = \frac{1}{2}\varrho g h \tag{32}$$

where $\varrho \equiv \rho(1-\rho/\rho_w)$, and we have used the boundary conditions at the calving front in Equation (4) to set the integration constant to zero.

6.2 Perturbations within the DV formulation

We begin with applying a small perturbation to the ice shelf, and assume that the ice dynamics can be described by a static density distribution as specified by the *Density Variations* [DV] formulation. This is a repeat of the analysis of section 5.2 but applied to a floating ice shelf. One of the key complications is that, unlike the reference solutions for a uniform ice sheet of constant thickness, the reference solutions for h and u vary with x. Additionally, the relationship between s and h is determined by the flotation condition in Equation (31) and so $\Delta h \neq \Delta s$.

In the DV formulation, the momentum and mass conservation equations describing the ice flow, Equations (32) and (2) respectively, become

$$\begin{aligned} 4\eta\partial_x u + \frac{2\eta}{\rho}u\partial_x\rho &= \frac{1}{2}\varrho g h \\ u\partial_x\rho + \rho(\partial_x u + \partial_z w) &= 0 \end{aligned}$$

and the kinematic boundary conditions are given by Equation (11). We apply a static perturbation to the density field, as described by Equations (7) and (8), with $\Delta\rho(x,t) = \mathcal{H}(t)\Delta\rho(x)$ and the reference density $\bar{\rho}$ is assumed to be spatially and temporarily constant. The momentum equation to zeroth-order is identically equal to the reference solution:

$$\partial_x \bar{u} = \frac{\bar{\varrho} g \bar{h}}{8\eta}$$

where $\bar{\varrho} \equiv \bar{\rho}(1-\bar{\rho}/\rho_w)$. While to first-order in the perturbations, the equations of motion are

$$\begin{aligned} 4\eta\partial_x\Delta u + \frac{2\eta}{\bar{\rho}}\bar{u}\mathcal{H}(t)\partial_x\Delta\rho &= \frac{1}{2}\bar{\varrho}g\Delta h + \frac{1}{2}g\bar{h}\mathcal{H}(t)\Delta\rho\left(2\frac{\bar{\varrho}}{\bar{\rho}} - 1\right) \\ \partial_z\Delta w &= -\partial_x\Delta u - \bar{u}\mathcal{H}(t)\frac{\partial_x\Delta\rho}{\bar{\rho}} \end{aligned} \tag{33}$$

The kinematic boundary conditions at the upper and lower surfaces to zeroth-order are

$$\begin{aligned} \bar{u}\partial_x\bar{s} - \bar{w}|_{\bar{s}} &= a_s \\ \bar{u}\partial_x\bar{b} - \bar{w}|_{\bar{b}} &= -a_b \end{aligned}$$

Notice the additional terms that arise due to the spatial variability of the reference solutions, $\bar{s}(x)$ and $\bar{b}(x)$. Nonetheless they still impose $\partial_z\bar{w}|_{\bar{s}} = \partial_z\bar{w}|_{\bar{b}} = 0$, since u is independent of depth in the SSA. Therefore, to first-order in the perturbations, and combining the two boundary conditions, we have

$$\Delta w|_{\bar{s}} - \Delta w|_{\bar{b}} = \partial_t\Delta h + \bar{u}\partial_x\Delta h + \Delta u\partial_x\bar{h} \tag{34}$$

We wish to solve the system of equations given by Equations (33) and (34). The spatially varying reference solutions, $\bar{h}(x)$ and $\bar{u}(x)$, mean that applying the Fourier transform as before would lead to convolution between variables in frequency space, which then no longer creates a linear system of equations. A direct solution of these differential equations is also not possible. Instead we turn to an approximation proposed in Ng et al. (2018). This approximation applies the Fourier and Laplace transforms to derive the transfer equations, under the assumption that the length scale for variation in the reference solution is much larger than that in the perturbations. In other words, we derive the transfer functions assuming that the reference solutions, $\bar{u}(x)$ and $\bar{h}(x)$, are locally constant. Under this assumption, the Fourier and Laplace transforms of Equations (33) and (34) are

$$\begin{aligned} -4ik\eta\Delta u - \frac{2ik\eta}{\bar{\rho}}\bar{u}r^{-1}\Delta\rho &= \frac{1}{2}\bar{\varrho}g\Delta h + g\bar{h}r^{-1}\Delta\rho\left(\frac{\bar{\varrho}}{\bar{\rho}} - \frac{1}{2}\right) \\ \partial_z\Delta w &= ik\Delta u + ik\bar{u}r^{-1}\frac{\Delta\rho}{\bar{\rho}} \\ \Delta w|_{\bar{s}} - \Delta w|_{\bar{b}} &= r\Delta h - ik\bar{u}\Delta h + \Delta u\partial_x\bar{h} \end{aligned}$$

where we have chosen to set the instantaneous response $\Delta h(t = 0^-) = 0$ as before. Notice that $\bar{u}$ and $\bar{h}$ continue to be functions of x, while Δu and Δh are functions of (k, r). Solving this system of equations, we arrive at the transfer function in the Laplace domain:

$$T_{h\rho}(k, x, r) = \frac{\Delta h}{\Delta \rho} = \frac{\bar{h}\left(\frac{1}{2}ik\bar{u}\phi^\star - \phi\left(2\partial_x\bar{u} - \beta\right)\right)}{r\bar{\rho}\left(r - p_{\mathrm{FL}}\right)}$$

where the dependence on x comes from the spatial variation of the background fields $\bar{h}$ and $\bar{u}$, and we have defined

$$\begin{aligned}
\beta &\equiv \frac{\bar{\rho}g\bar{h}}{8\eta} \\
\phi &\equiv 1 - \frac{\partial_x\bar{h}}{ik\bar{h}} \\
\phi^\star &\equiv 1 + \frac{\partial_x\bar{h}}{ik\bar{h}} \\
p_{\mathrm{FL}} &\equiv ik\bar{u} - \phi\partial_x\bar{u}
\end{aligned}$$

We can convert back into the time-domain through the inverse Laplace transform. The function has two poles at $r = 0$ and $r = p_{\mathrm{FL}}$. For the reference solution $\partial_x\bar{u} > 0$, and so the pole defined by $r = p_{\mathrm{FL}}$ will reside in the left half of the complex plane, the same as in previous solutions. We arrive at

$$T_{h\rho}(k, x, t) = \frac{\bar{h}\left(\frac{1}{2}ik\bar{u}\phi^\star - \phi\left(2\partial_x\bar{u} - \beta\right)\right)}{\bar{\rho}p_{\mathrm{FL}}}\left(e^{p_{\mathrm{FL}}t} - 1\right) \tag{35}$$

Numerical integration is required to transform this from the frequency domain into the spatial domain. Following the procedure in Ng et al. (2018), the transformation into the spatial domain is slightly different to that described in Equation (19). The thickness perturbation in the Fourier-domain is given by

$$\Delta h(k, t) = \int_{-\infty}^{\infty} T_{h\rho}(k, x, t)\Delta\rho(x)e^{ikx}\mathrm{d}x$$

and taking the inverse Fourier transform, we arrive at the thickness perturbation, $\Delta h(x, t)$.

We can also follow a similar procedure to find the response of the horizontal velocity to perturbations in the density:

$$T_{u\rho}(k, x, t) = \frac{-\bar{u}\left(\frac{1}{2}ik\bar{u} + \partial_x\bar{u} - \beta\right)}{\bar{\rho}p_{\mathrm{FL}}} - \frac{\partial_x\bar{u}\left(\frac{1}{2}ik\bar{u}\phi^\star - \phi\left(2\partial_x\bar{u} - \beta\right)\right)}{ik\bar{\rho}p_{\mathrm{FL}}}e^{p_{\mathrm{FL}}t} \tag{36}$$

The first term in this transfer function is the steady-state response, which for small wavelengths tends to $-\bar{u}/2\bar{\rho}$ and for large wavelengths tends to zero. While the second term is a transient component which decays over time. For small wavelengths it tends to zero, but for large wavelengths ($k \to 0$) it scales as $1/k$ and tends to infinity. This spurious behaviour arises because the derivation of the transfer function relied on a separation of scales between the perturbation and the background steady-state, which breaks down at very large wavelengths. If $\partial_x\bar{u}$ and $\partial_x\bar{h} = 0$, then the term would disappear. It is important to filter out these very large wavelength contributions in any perturbations that are applied. In the simulations that follow in section 7, we set the lowest frequency component of the transfer function to zero, so that the numerical integration is well-behaved.

6.3 Perturbations within the DV-BF formulation

If we follow the same procedure, but ignore the term in $D\rho/Dt$ on the left hand side of the momentum equation, as described by the *Density Variations - Body Force*

only [DV-BF] formulation, then the momentum and mass conservation equations describing the ice flow, Equations (32) and (2) respectively, become

$$\begin{aligned} 4\eta\partial_x u &= \frac{1}{2}\varrho g h \\ u\partial_x\rho + \rho(\partial_x u + \partial_z w) &= 0 \end{aligned}$$

and the derived transfer functions are

$$T_{h\rho}(k,x,t) = \frac{\bar{h}\left(ik\bar{u} - \phi\left(2\partial_x\bar{u} - \beta\right)\right)}{\bar{\rho}p_{\mathrm{FL}}}\left(e^{p_{\mathrm{FL}}t} - 1\right) \tag{37}$$

$$T_{u\rho}(k,x,t) = \frac{-\bar{u}\left(\partial_x\bar{u} - \beta\right)}{\bar{\rho}p_{\mathrm{FL}}} - \frac{\partial_x\bar{u}\left(ik\bar{u} - \phi\left(2\partial_x\bar{u} - \beta\right)\right)}{ik\bar{\rho}p_{\mathrm{FL}}}e^{p_{\mathrm{FL}}t} \tag{38}$$

6.4 Perturbations within the DVA formulation

In this next example, we assume the ice dynamics can be described by an initial density distribution which then advects over time as specified by the *Density Variations Advected* [DVA] formulation. We follow the procedure in section 5.4 closely but this time applied to the reference state of a floating ice shelf.

In the DVA formulation, the equations of motion describing the ice flow, from Equations (32), (2) and (23) respectively, are

$$\begin{aligned} 4\eta\partial_x u &= \frac{1}{2}\varrho g h \\ \partial_x u + \partial_z w &= 0 \\ \partial_t\rho + u\partial_x\rho &= 0 \end{aligned}$$

We apply a perturbation to the density field which can evolve over time as described in Equations (7) and (8) with $\Delta\rho(x, t < 0) = 0$. The kinematic boundary conditions are the same as we had before in Equation (34). Keeping terms to first-order and applying the Fourier and Laplace transforms, as described in section 6.2 for spatially variable reference states, we arrive at the following system of equations:

$$\begin{aligned} -4ik\eta\Delta u &= \frac{1}{2}\bar{\varrho}g\Delta h + \frac{1}{2}g\bar{h}\Delta\rho\left(2\frac{\bar{\varrho}}{\bar{\rho}} - 1\right) \\ \partial_z\Delta w &= ik\Delta u \\ \Delta w|_{\bar{s}} - \Delta w|_{\bar{b}} &= r\Delta h - ik\bar{u}\Delta h + \Delta u\partial_x\bar{h} \\ r\Delta\rho - \Delta\rho_0 &= ik\bar{u}\Delta\rho \end{aligned}$$

where $\Delta\rho_0 \equiv \Delta\rho(k, t = 0)$, and as before we have chosen to set $\Delta h(t = 0^-) = 0$. This system of equations can be solved to arrive at an expression for the transfer function in the Laplace-domain:

$$T_{h\rho_0}(k,x,r) \equiv \frac{\Delta h}{\Delta\rho_0} = \frac{-\bar{h}\phi\left(2\partial_x\bar{u} - \beta\right)}{\bar{\rho}\left(r - p_{\mathrm{FL}}\right)\left(r - ik\bar{u}\right)}$$

Applying the inverse-Laplace this can be converted to the time-domain, and after some simplification, we arrive at

$$T_{h\rho_0}(k,x,t) = \bar{h}\left(\frac{2}{\bar{\rho}} - \frac{1}{\bar{\varrho}}\right)\left(e^{p_{\mathrm{FL}}t} - e^{ik\bar{u}t}\right) \tag{39}$$

We can also follow a similar procedure to find the response of the horizontal velocity to perturbations in the *initial* density field:

$$T_{u\rho_0}(k,x,t) = \frac{-\left(2\partial_x\bar{u} - \beta\right)}{ik\bar{\rho}}e^{p_{\mathrm{FL}}t} \tag{40}$$

6.5 Perturbations within the D2T formulation

Finally, we repeat the perturbation analysis for a floating ice shelf, but assume the ice-flow can be described by the *Density-to-Thickness Adjustment* [D2T] formulation. This follows closely a combination of the procedures in section 5.5 and section 6.2.

In the D2T formulation, the momentum-conservation described by Equation (32) becomes

$$4\eta\partial_x u = \frac{1}{2}\rho_{\text{ice}} g(h-\delta)\left(1-\frac{\rho_{\text{ice}}}{\rho_w}\right)$$

which can be expressed in terms of the vertically-averaged density as

$$4\eta\partial_x u = \frac{1}{2}\rho g h\left(1-\frac{\rho_{\text{ice}}}{\rho_w}\right)$$

The mass-conservation and kinematic boundary conditions are given by Equations (27) and (28) respectively. We apply a static perturbation to the density field, as described by Equations (7) and (8), with $\Delta\rho(x,t) = \mathcal{H}(t)\Delta\rho(x)$. Unlike in all the previous configurations, the zeroth-order solution to the momentum equation is not identically equal to the reference solution given by Equation (C1). We have a slight shift in the equilibrium profile of the floating ice shelf:

$$\partial_x \bar{u} = \frac{\bar{\rho} g \bar{h}}{8\eta}\left(1-\frac{\rho_{\text{ice}}}{\rho_w}\right)$$

which vanishes if the background density is equal to that of pure ice. Keeping terms to first-order and applying the Fourier and Laplace transforms as described in section 6.2 for spatially variable reference states, we arrive at the following system of equations:

$$\begin{aligned}
-4ik\eta\Delta u &= \frac{1}{2}g\left(\bar{\rho}\Delta h + \bar{h}r^{-1}\Delta\rho\right)\left(1-\frac{\rho_{\text{ice}}}{\rho_w}\right)\\
\partial_z \Delta w &= ik\Delta u\\
\Delta w|_{\bar{s}-\bar{\delta}} - \Delta w|_{\bar{b}} &= (r-ik\bar{u})\frac{\bar{\rho}}{\rho_{\text{ice}}}\Delta h - ik\bar{u}r^{-1}\frac{\bar{h}}{\rho_{\text{ice}}}\Delta\rho + \frac{\bar{\rho}}{\rho_{\text{ice}}}\partial_x\bar{h}\Delta u
\end{aligned}$$

where again with the D2T adjustment approach, the density perturbation gets applied *before the run starts*, and so $\Delta s(t=0^-) = 0$, but effectively $\mathcal{H}(t=0^-) = 1$, as discussed in section 5.5. Following the same steps as before, we arrive at the transfer function,

$$T_{h\rho}(k,x,r) \equiv \frac{\Delta h}{\Delta\rho} = \frac{\bar{h}\tilde{p}_{\text{FL}}}{\bar{\rho}r\left(r-\tilde{p}_{\text{FL}}\right)}$$

where we have defined

$$\tilde{p}_{\text{FL}} \equiv ik\bar{u} - \beta\phi\left(1-\frac{\rho_{\text{ice}}}{\rho_w}\right)$$

Taking the inverse Laplace, we arrive at

$$T_{h\rho}(k,x,t) = \frac{-\bar{h}}{\bar{\rho}}\left(1-e^{\tilde{p}_{\text{FL}}t}\right) \tag{41}$$

This is identical to the transfer function derived in Equation (29) for the D2T adjustment in the context of a grounded ice sheet, just with an adjusted pole $\tilde{p}_{\text{FL}}$. Again, this leads to a constant transfer function at all frequencies in the steady-state.

We can also follow a similar procedure to find the response of the horizontal velocity to perturbations in the density:

$$T_{u\rho}(k,x,t) = -\beta\left(1-\frac{\rho_{\text{ice}}}{\rho_w}\right)\frac{1}{ik\bar{\rho}}e^{\tilde{p}_{\text{FL}}t} \tag{42}$$

7 Comparing the Perturbation Analysis Results

The transfer functions derived in the previous two sections, which describe the response of the ice sheet to small perturbations in the ice density, have given us a number of insights into the different density formulations proposed in section 3. In this section we summarise the results and analyse their implications.

7.1 The Steady-State Solutions with Uniform Density

In sections 5.1 and 6.1, we derived the equilibrium solutions for the ice-flow with constant density for two reference configurations: a grounded ice sheet, and a floating ice shelf. We would expect this to be the same as the zeroth-order solution within the perturbation analysis for each of the density formulations. For the grounded ice sheet, this is indeed the case, with the zeroth-order D2T solution the same as for all the other density approaches. In all cases,

$$\bar{u} = c\left(\bar{\rho} g \bar{h} \sin\alpha\right)^m$$

The reference velocity scales as $\rho \times h$, a quantity which is preserved in the D2T adjustment, and so this agreement is perhaps not surprising. However, for the floating ice shelf, the D2T zeroth-order momentum equation is

$$\partial_x \bar{u} = \frac{\bar{\rho} g \bar{h}}{8\eta}\left(1 - \frac{\rho_{\text{ice}}}{\rho_w}\right) \tag{43}$$

whereas in the other density formulations we have

$$\partial_x \bar{u} = \frac{\bar{\rho} g \bar{h}}{8\eta}\left(1 - \frac{\bar{\rho}}{\rho_w}\right) \tag{44}$$

where all variables refer to the same physical quantities. Therefore, in a situation without horizontal density variations, but in which the average density is less than pure ice (i.e. the same proportion of firn everywhere), we find that the velocity field will be inaccurate when estimated from a simulation which uses the D2T adjustment. To understand how this arises, consider the flotation condition obeyed by an ice shelf, in which the weight of the water displaced equals the weight of the ice-column above. In the D2T adjustment, the weight of the ice-column is preserved and so the amount of water displaced is the same, which means that the location of the lower surface b is unchanged. However, in the D2T adjustment, the thickness of the ice shelf is reduced if the average density is less than that of pure ice. This means that the upper surface s is shifted downwards. The thickness of the ice shelf decreases with distance from the grounding line, and so a constant average density implies a decreasing firn air-content $\delta(x)$ with distance from the grounding line. Therefore, the D2T adjustment is largest close to the grounding line, and as such the gradient of the upper surface $\partial_x s$ is smaller in the D2T adjustment formulation. This is one of the many factors influencing the velocity field (and ultimately the thickness profile) and leads to a slightly different equilibrium state for the floating ice shelf in the D2T formulation.

7.2 The Transfer Functions

In Tables 1 and 2, we summarise the transfer functions derived in sections 5 and 6 for the grounded ice sheet and floating ice shelf respectively, in the limit as $t \to \infty$. The transfer functions have a steady-state component (summarised here) as well as a time component which decays exponentially. The transfer functions describe the amplitude and phase of the induced perturbations in the thickness and velocity fields as a function of the wavelength of the applied density perturbation. The analytical transfer functions derived in this study are valid for wavelengths of one ice-thickness or greater ($\lambda > \bar{h}$), otherwise the validity of the SSA breaks down. In the case of the floating ice shelf,

Table 1. Normalised steady-state transfer functions for induced perturbations in the ***glacial thickness*** in response to an initial density perturbation: $T_{h\rho}(k,t) \times \left(\frac{-\bar{\rho}}{\bar{h}}\right)$. Note, for the grounded ice sheet $\Delta h = \Delta s$, and so $T_{h\rho} = T_{s\rho}$.

	GROUNDED ICE-SHEET	FLOATING ICE-SHELF
Density Variations [DV]:	$\frac{p + \frac{1}{2}t_r^{-1} - ik\bar{u}\zeta}{p}$	$\frac{\frac{1}{2}ik\bar{u}\phi^\star - \phi\left(2\partial_x\bar{u} - \beta\right)}{p_{\mathrm{FL}}}$
Density Variations (body force term only) [DV-BF]:	$\frac{p + \frac{1}{2}t_r^{-1}}{p}$	$\frac{ik\bar{u} - \phi\left(2\partial_x\bar{u} - \beta\right)}{p_{\mathrm{FL}}}$
Density Variations Advected [DVA]:	$\frac{p - ik\bar{u} + \frac{1}{2}t_r^{-1}}{p - ik\bar{u}}e^{ik\bar{u}t}$	$\frac{-\phi\left(2\partial_x\bar{u} - \beta\right)}{p_{\mathrm{FL}} - ik\bar{u}}e^{ik\bar{u}t}$
Density Variations translated to thickness adjustment [D2T]:	1	1

we have the additional restriction that the wavelength must be less than the scale of variation in the background fields for the method to be valid. This restricts $k < \partial_x\bar{h}/\bar{h}$ and $k < \partial_x\bar{u}/\bar{u}$. The steady-state transfer functions for a grounded ice sheet are plotted in Figure 2, and for a floating ice shelf in Figure 3. For the grounded ice sheet, results are shown for two different slipperiness values, and for the floating ice shelf for two different horizontal velocities. There are clear qualitative and quantitative differences between the four different density formulations that we have studied.

One notable difference is that within the D2T adjustment formulation, the steady-state transfer function describing the amplitude transfer between the density perturbations and induced perturbations in the thickness, is equal to unity independently of wavelength. The other density formulations are more nuanced in their frequency response and dependent on the flow characteristics. For example, the induced surface perturbations are dampened at small wavelengths for many of the density formulations. On the other hand, in the case of a floating ice shelf, the amplitude of the induced thickness perturbations, particularly at larger wavelengths and slower flows, is amplified to be larger than that of the initial density perturbation. Comparing the behaviour of the DV and DV-BF formulations, we see that the transfer functions are more similar at larger wavelengths, and are a particularly close match for less-slippery grounded topography. This makes sense, since as the slipperiness decreases the basal drag dominates on the left hand side of the momentum equation, and the additional density correction term becomes less significant, as discussed in section 4. Note that for very small wavelengths the SSA breaks down and we care less about the discrepancy between different methods.

In both the D2T adjustment and DVA formulations, the perturbation in the ice velocity field decays over time to zero across all wavelengths. This is a consequence of the advection of the density perturbation with the ice-flow. This advection is explicit in the DVA formulation, but implicit in the D2T adjustment method. In the D2T method, the density perturbation is translated to a perturbation in the adjusted *ice-equivalent*

Table 2. Normalised steady-state transfer functions for induced perturbations in the ***horizontal velocity*** in response to an initial density perturbation: $T_{u\rho}(k,t) \times \left(\frac{-\bar{\rho}}{\bar{u}}\right)$.

	GROUNDED ICE-SHEET	FLOATING ICE-SHELF
Density Variations [DV]:	$\frac{\left(\frac{1}{2}t_r^{-1} - ik\bar{u}\zeta\right)}{p}$	$\frac{-\left(\frac{1}{2}ik\bar{u} + \partial_x\bar{u} - \beta\right)}{p_{\mathrm{FL}}}$
Density Variations (body force term only) [DV-BF]:	$\frac{\frac{1}{2}t_r^{-1}}{p}$	$\frac{-\left(\partial_x\bar{u} - \beta\right)}{p_{\mathrm{FL}}}$
Density Variations Advected [DVA]:	0	0
Density Variations translated to thickness adjustment [D2T]:	0	0

surface which then dissipates over time. Consequently, the velocity perturbation tends to zero in the steady-state. However, the steady-state D2T thickness transfer function does not approach zero, because we add the initial density perturbation back onto the adjusted surface to find the *unmodified* surface at the end of the simulation.

7.3 Transient Response to a Perturbation

The transfer functions allow us to now calculate the transient flow response to a prescribed initial perturbation in density. In Figures 4 and 5, we have plotted the evolution of the surface and velocity in response to a 10% Gaussian perturbation in the density field, for the grounded ice sheet and floating ice shelf respectively. As discussed in section 7.1, the zeroth-order solution for a floating ice shelf with the D2T adjustment applied (Equation (43)) is slightly different to that in the other density formulations. Here we are focusing on the first-order contribution from small perturbations and so we have plotted the D2T perturbation relative to the zeroth-order solution in the other formulations (Equation (44)) to aid comparison.

For the grounded ice sheet of Figure 4, the surface is initially unperturbed, and then as the ice flows through this more dense region, a surface depression is formed at the location of the density perturbation. Note that in the context of the D2T formulation, we are referring to the *unmodified* surface, where the initial density perturbation is added back on to the ice-equivalent surface in the model as a corresponding thickness perturbation. This depression travels with the ice-flow in the case of the DVA (density variations advected) formulation, but for the static DV, DV-BF and D2T formulations it stays fixed. The depression is most pronounced in the D2T adjustment method, whereas there is some damping of the perturbation in the other density formulations. As the ice flows through the density perturbation, a kinematic wave is formed at the surface travelling at a phase speed of ω/k, where the angular frequency ω is equal to the imaginary part of the exponent of the transfer function $T_{s\rho}(k,t)$ in Equations (18, 21, 24 & 29). This phase speed is identical across all the density formulations (the slight correction due to

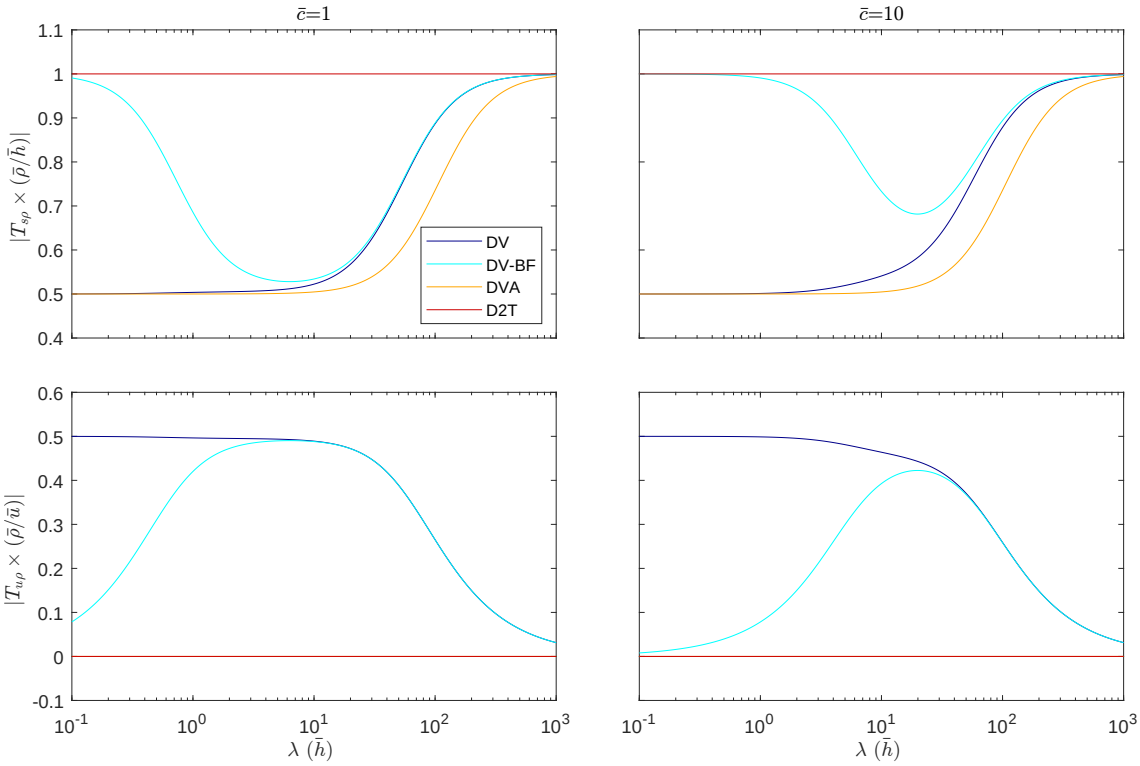

Figure 2. Steady-state transfer functions for the grounded ice sheet, showing the impact of horizontal density variations on surface topography (upper panel) and horizontal velocity (lower panel). The scales are chosen such that the mean thickness, basal shear stress, and deformational velocity are all set to unity, i.e. $\bar{h} = 1$, $g = 1/\bar{\rho}\bar{h}\sin\alpha$ and $\eta = 0.5$. Additionally we set $\alpha = 3°$, $\bar{\rho} = 792$, $m = 1$, and consider two choices of mean slipperiness: $c = 1$ (LHS) and $c = 10$ (RHS). The wavelength is in units of $\bar{h}$. Note the DVA line is obscured behind the D2T line in the lower panel plots.

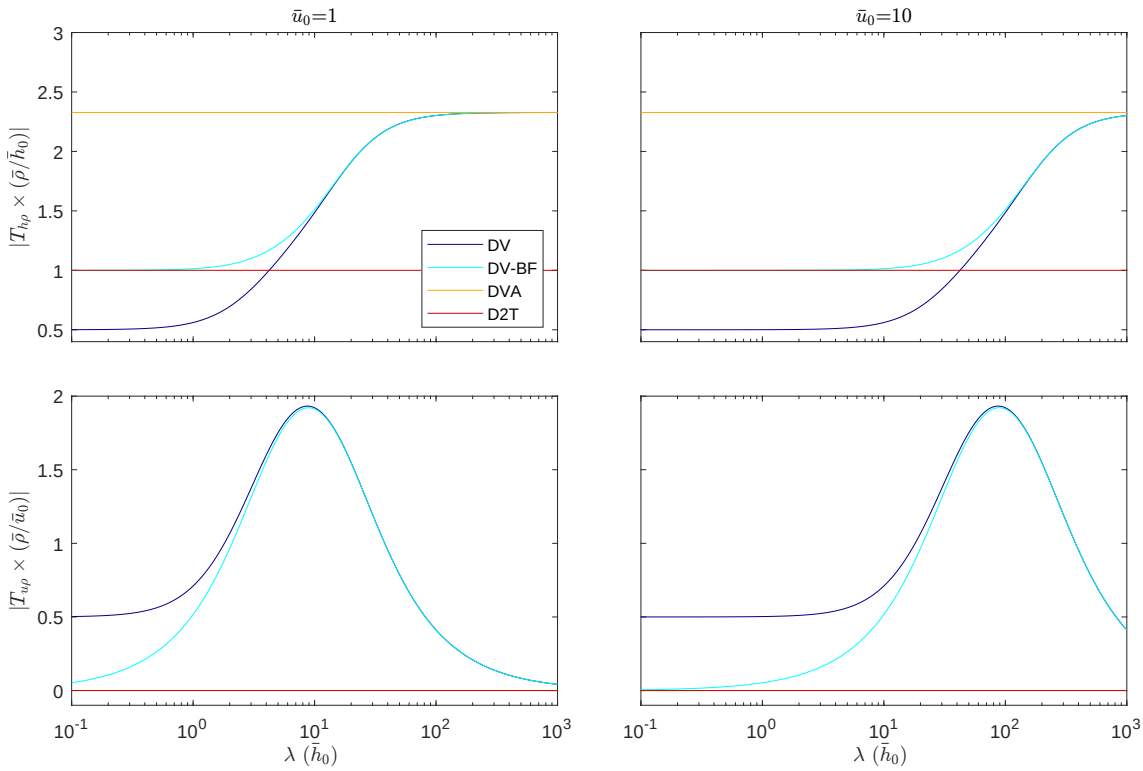

Figure 3. Steady-sate transfer functions for the floating ice shelf, showing the impact of horizontal density variations on ice-shelf thickness (upper panel) and horizontal velocity (lower panel). The transfer functions are spatially-dependent; here we consider the transfer functions at a particular spatial coordinate for which $\bar{h}(x) = \bar{h}_0$ and $\bar{u}(x) = \bar{u}_0$. The scales are chosen such that the mean thickness, horizontal deviatoric stress and strain rate are all set to unity, i.e. $\bar{h}_0 = 1$, $g = 4/\bar{\varrho}\bar{h}_0$ and $\eta = 0.5$. Additionally we set $\alpha = 3°$, $\bar{\rho} = 792$, $a = 0.5$ and consider two choices for the horizontal velocity: $\bar{u}_0 = 1$ (LHS) and $\bar{u}_0 = 10$ (which impacts the solution through $\partial_x \bar{h}$). The wavelength is in units of $\bar{h}_0$. Note the DVA line is obscured behind the D2T line in the lower panel plots.

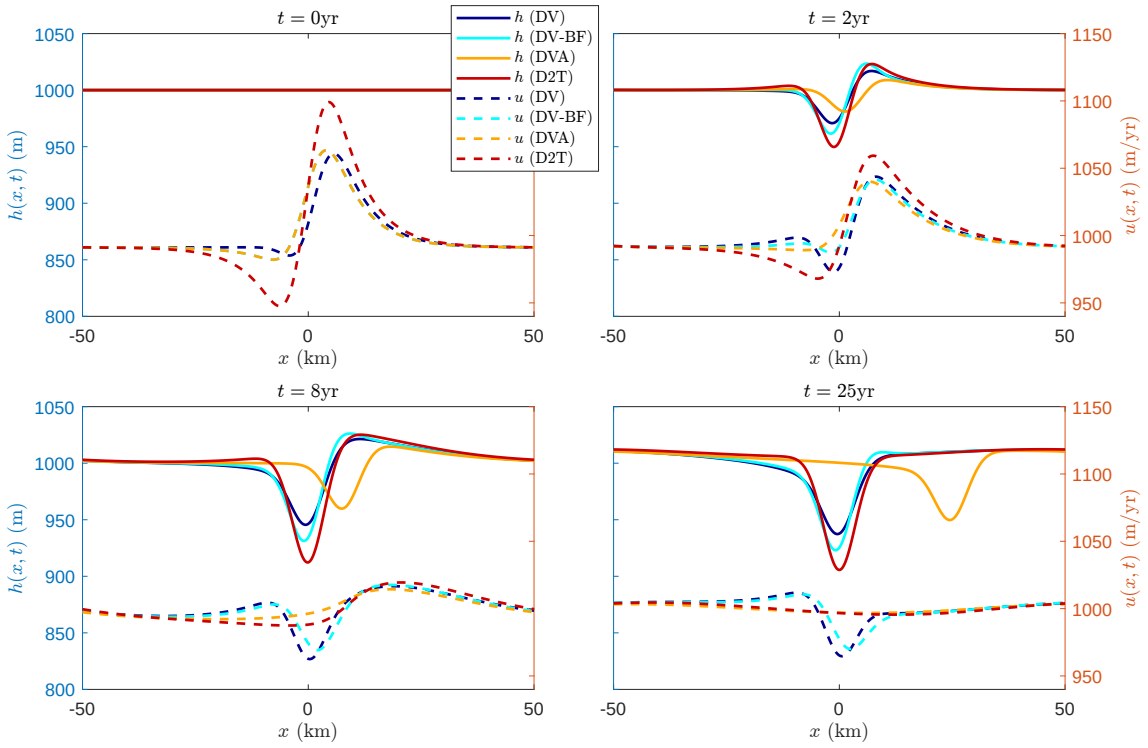

Figure 4. Example of the evolution of the spatial distribution in $h(x,t)$ [solid lines] and $u(x,t)$ [dashed lines] after an initial 10% Gaussian density perturbation applied in $\Delta\rho$, for the grounded ice sheet. This compares the analytical responses across the four different approaches for handling density evolution. See the body of the text for a description of the four methods. In this simulation, we set $\alpha = 3°$, $\bar{\rho} = 900\,\mathrm{kg/m^3}$, $m = 1$, $\eta = 5 \times 10^3\,\mathrm{kPa \cdot yr}$ and $\bar{u} = 1000\,\mathrm{m/yr}$.

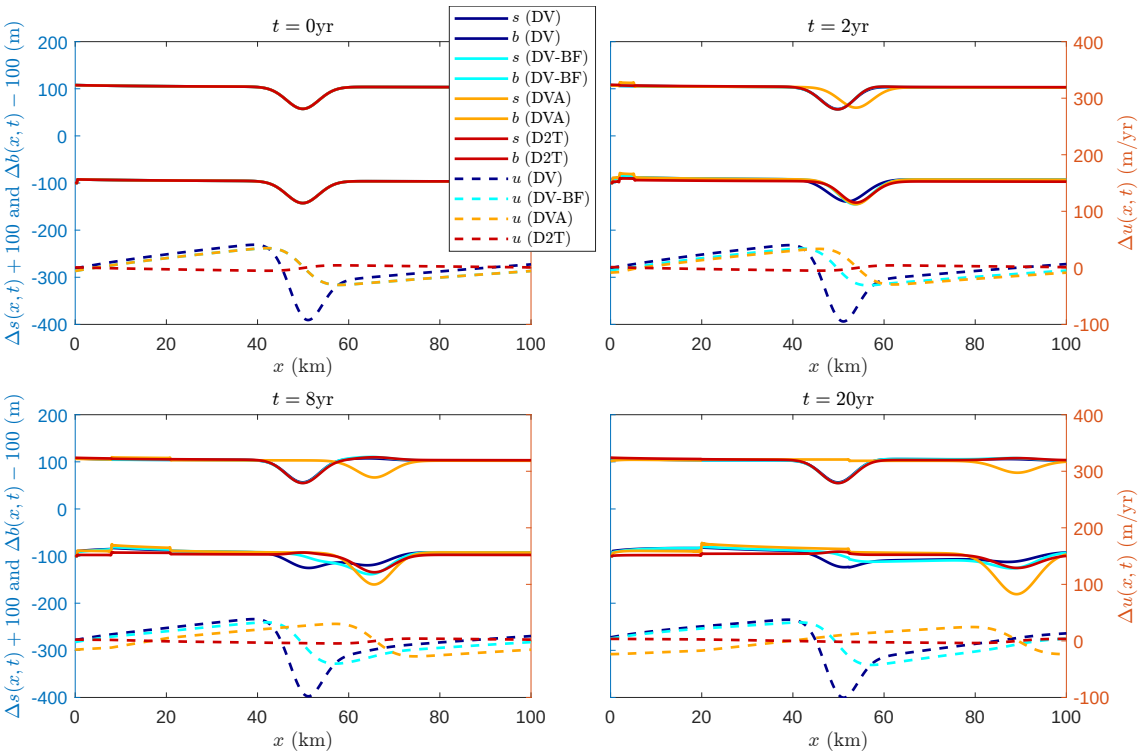

Figure 5. Example of the evolution of the spatial distribution in the upper and lower surfaces, $s(x,t)$ and $b(x,t)$ [solid lines], and velocity, $u(x,t)$ [dashed lines], after an initial 10% Gaussian density perturbation applied in $\Delta\rho$, for the floating ice shelf. The perturbed surfaces and velocity are plotted relative to their equilibrium values (plotted in Figure C1), with the upper and lower surfaces offset by $\pm$100m to separate them. This compares the analytical responses across the four different approaches for handling density evolution. See the body of the text for a description of the four methods. In this simulation, we set $\bar{\rho} = 900\,\mathrm{kg/m^3}$, $\eta = 5 \times 10^3\,\mathrm{kPa \cdot yr}$ and the surface accumulation $a_s = 1\,\mathrm{m/yr}$. Note the sight glitches in the lower surface in the unperturbed region to the left of each plot are just an artefact of the numerical integration in the DVA approach.

$\bar{\rho}$ vs ρ_{ice} in the D2T method is negligible), and equals

$$\frac{\omega}{k} = \bar{u} + \tau_d \xi^{-1} = \bar{u} + \frac{m\bar{u}}{1 + 4\bar{h}\eta k^2/\gamma}$$

The wavelength dependency of the phase speed causes the kinematic wave to disperse as it propagates. In the limit of small and large wavelengths, the phase speed tends to $\bar{u}$ and $(m+1)\bar{u}$ respectively. In general a surface disturbance will propagate at the group velocity, given by $d\omega/dk$. In the DVA formulation, there is an additional transient component in the transfer function in Equation (24), with a phase speed which travels with the advecting of the density perturbation: $\omega/k = \bar{u}$. In the example in Figure 4, this phase speed is 1000 m/yr, which is in excellent agreement with the apparent propagation of the surface depression in the figure.

For the floating ice shelf of Figure 5, the initial density perturbation immediately causes a depression in the ice due to the flotation condition, which requires more water be displaced to counteract the weight of the heavier ice. This depression dissipates in the lower surface, but persists in the upper surface due to the flotation condition, and stays fixed in the DV, DV-BF and D2T formulations. The perturbation generates a kinematic wave, which is most visible in the lower surface (since flotation dictates that $\Delta s \approx 0.1\Delta b$). From the transfer functions in Equations (35, 37, 39 & 41), the phase speed of the kinematic wave is

$$\frac{\omega}{k} = \bar{u} - \frac{\partial_x \bar{u}}{k^2 \bar{h}}$$

Again, the dependency of the phase speed on wavelength results in dispersion of the wave. In the DVA formulation, the additional transient component describing the propagation of the surface depression itself also has a phase speed equal to $\bar{u} = 2000$ m/yr, for the parameters used in the experiment in Figure 5, consistent with the apparent propagation of the depression.

These simulations show some broad patterns of similarity between the different approaches for including HDVs in ice-flow models, but also some important qualitative differences. In the D2T adjustment, the density perturbation is applied to the *adjusted* surface from which it then dissipates, which means the velocity profile is a closer match to that of the advecting (DVA) formulation. However, to arrive at the *unmodified* surface (which is what we plotted here), the initial density perturbation must be added back onto the *adjusted* surface, and so the surface response in the D2T formulation is a closer match to that of the DV or DV-BF formulations. For all simulations, the DV and DV-BF formulations produce similar results, although not identical. The relative significance of the additional density correction term, present in the DV but not the DV-BF formulation, depends on the topography as discussed in section 4. In this example, the high frequency components in the Gaussian perturbation may increase the impact of this term, and exaggerate the differences between the DV and DV-BF formulations.

For all these examples, with the exception of the DVA formulation, we compared the analytical response calculated from the transfer functions (plotted in Figures 4 and 5 above), to numerical simulations implemented in the ice-flow model Úa. The details are provided in Appendix D. We found an excellent agreement which gives us confidence in the derived transfer functions. The results for the floating ice shelf are particularly pleasing since they rely on the approximation presented in Ng et al. (2018) to derive the analytical transfer functions, which confirms the validity of this approximation.

8 Numerical Simulations of Antarctica

In the preceding sections, we have extensively analysed the behaviour of the ice flow within a theoretical framework for the four different density formulations proposed in section 3: *Density-to-Thickness adjustment* (D2T), *Density Variations* (DV), *Density*

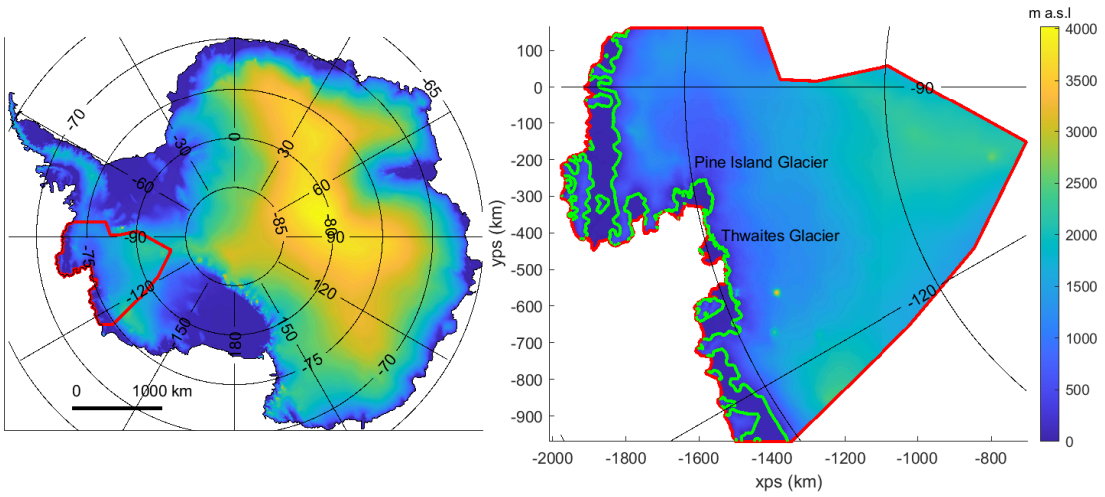

Figure 6. Surface elevation of the Pine Island glacier and Thwaites glacier region in Antarctica. Our domain is outlined in red; the grounding line in bright green.

Variations - Body Force only (DV-BF), and *Density Variations Advected* (DVA). In this section we investigate the impact of horizontal density variations (HDVs) in a real-world setting, and focus on the two approaches for including HDVs which are used in current ice-flow models. The first is the DV-BF formulation, which is the default implementation in Úa. This incorporates a static density distribution, with horizontal density gradients included in the body-force driving term of the SSA momentum equation. The second formulation is the D2T adjustment method which is the default in many ice-flow models, and requires no adjustment to the standard SSA equations. It is simple to implement, only requiring an adjustment to the initial ice-thickness distribution.

We use the shallow-ice model Úa (Gudmundsson, 2020b) for these simulations, and focus on the Pine Island and Thwaites glaciers in the Western Antarctic, a region which has suffered some of the most rapid mass-loss in the Antarctic (Rignot et al., 2019; Shepherd et al., 2018). The computational domain is outlined in Figure 6. In addition to the DV-BF and D2T methods, we include a simulation where the density is assumed constant throughout the ice sheet, but the height is set at the thickness of the ice sheet, without any D2T adjustment. We refer to this method as *No Variations* [NV]. We choose an average density $\rho = 900\,\mathrm{kg/m^3}$ everywhere, which minimises the grounding line mismatch in the simulation domain.

We follow the approach taken in recent simulation studies of this region, such as in Barnes et al. (2021) and De Rydt et al. (2021). The geometry of the Western Antarctic Ice Sheet was taken from the BedMachine Antarctica dataset (Morlighem, 2020; Morlighem et al., 2020), which includes estimates of the *firn air-content*, δ. The firn correction is applied by default to the thickness published in the BedMachine Antarctica dataset. The varying density of the Western Antarctic Ice Sheet can be extracted from the firn air-content and is plotted in Figure 7, together with measurements of surface velocity extracted from Gardner, Moholdt, et al. (2018). Model parameters relating to the rheology of ice (rate factor A) and basal sliding conditions (slipperiness C) were selected using a model inversion. The inversion depends on two regularisation parameters. A previous study by Barnes et al. (2021) looked in detail at inversion methods used in three different ice-flow models, including Úa. The authors performed an L-curve analysis to find the optimal trade-off between minimising the misfit and regularisation terms in the cost function. We utilise the regularisation parameters found in that study: $\gamma_a = 1$, $\gamma_s =$

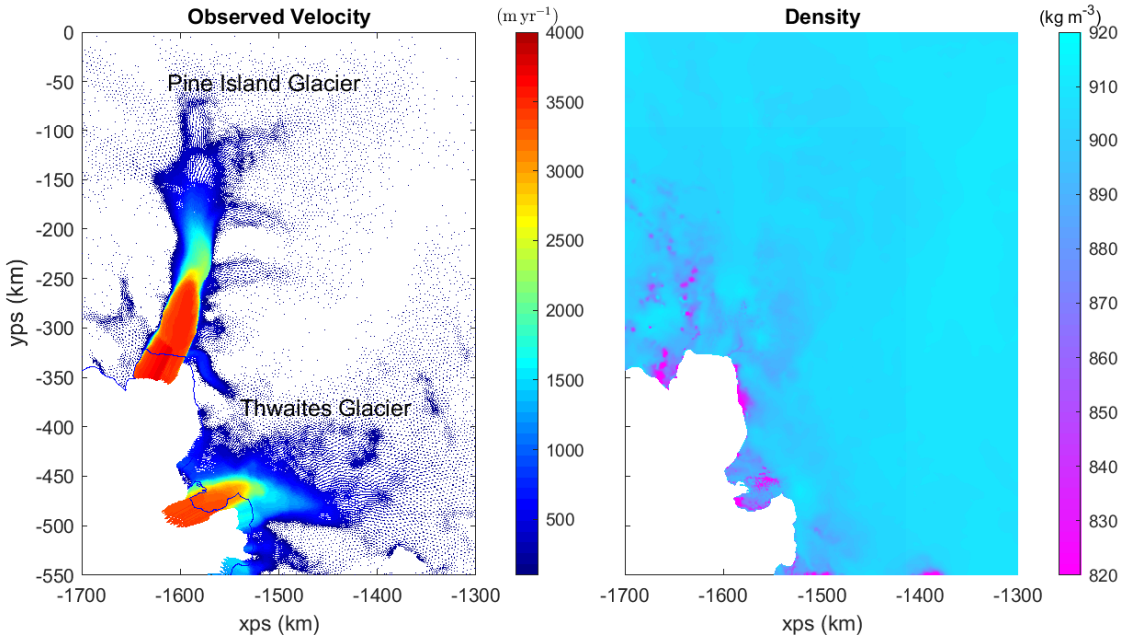

Figure 7. The observed velocities and density variation for the Western Antarctic around the Pine Island and Thwaites glaciers.

10^4. See Barnes et al. (2021) for a comprehensive description of these parameters. We assume a common choice for the creep exponent in Glen's flow law, $n = 3$ which describes the ice rheology, and similarly set the exponent $m = 3$ in Weertman's sliding law to describe the basal sliding.

It is important to note that the inversion products, A and C, are not unique to the domain. The inversion process selects the A and C fields which are consistent with the geometry, observed velocity fields and forward ice-flow model. Between each of the density formulations, the forward model is slightly different, and so each formulation requires a slightly different A and C field to recover the observed velocities in the Antarctic domain. Therefore within each of the simulations for the three different density approaches (DV-BF, D2T and NV), we optimise for A and C separately. This separate inversion for A and C is essential to ensure that the difference in sea level estimates is coming from the different ice-flow dynamics in the different density formulations, as opposed to different initial velocities. After a diagnostic run, the model velocities are a close match to the observed surface velocities in each of the approaches, suggesting that any difference in the model dynamics due to different density formulations can, initially, be compensated for through optimisation of other model parameters. The real test of the impact of including density variations in the model is the evolution of the ice flow over a significant period of time.

When performing a time-dependent run, the model also requires inputs for the estimated surface mass-balance, and applied basal melting. Similar to other studies in this region, the surface mass-balance is derived from the Regional Climate Model (Van Wessem et al., 2014, RACMO v2.3). However, the basal melt is more difficult to infer. An estimate can be made from principles of mass-conservation, together with observations of grounding line retreat in the region. Within each simulation, we calculate the changes in volume above flotation (VAF) over a 40 year period, and compare the results between the different formulations for including HDVs. This is plotted in Figure 8, together with the corresponding change in sea level. Over a 40yr horizon the variation between the dif-

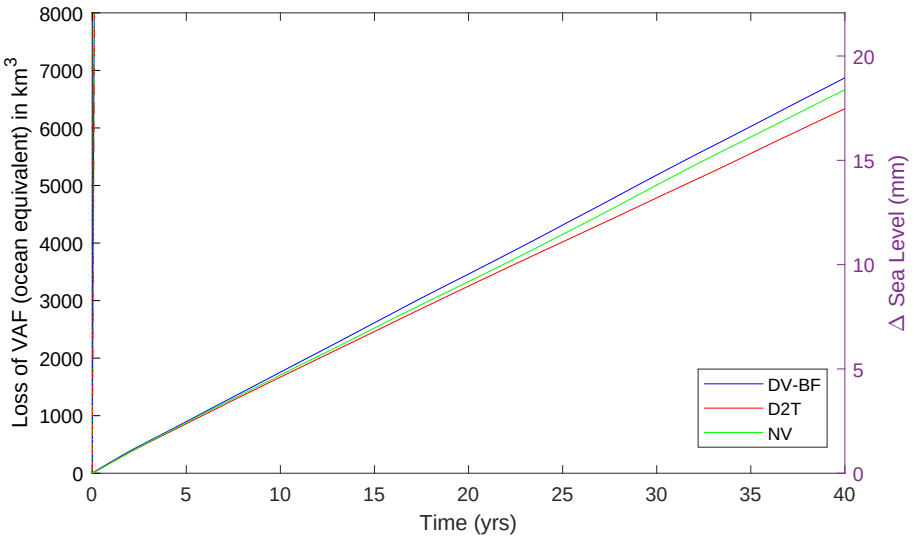

Figure 8. The change in Volume Above Flotation (VAF) for the model domain in the Western Antarctic, and corresponding sea level rise, for each of the density formulations we consider here.

ferent density formulations is approximately 2mm, a 10% correction to the overall estimate of sea level rise, with the DV-BF formulation leading to the largest estimates of ΔVAF. We ran a number of simulations to confirm that the impact was relatively insensitive to some of the modelling choices we made. For example, a reduction in the applied basal melting leads to significantly less total mass-loss, but similar absolute difference in ΔVAF between the different configurations. In Figure 9, we also plot the model velocities and grounding line position at the end of the 40yr run for each of the density formulations. While the grounding line positions are roughly identical between each of the simulations, the velocity fields in the fast flowing regions of the Pine Island and Thwaites ice-shelves show subtle differences. We see slightly higher velocities in the central fast-flowing region of the Pine Island ice shelf and Thwaites Eastern tongue for the DV-BF compared to the D2T formulation. The slightly reduced velocity in the D2T formulation is in keeping with the lower estimates of sea level rise.

In summary, we find that for the particular case of the West Antarctic Ice Sheet and using a model setup typical of many recent ice-flow modelling studies, the inclusion of horizontal density variations by adjusting the thickness (D2T) as commonly done, compared to adjusting the body-force term in the momentum equation (DV-BF), leads to about a 10% change in the sea level contribution of that area over 40 years.

9 Conclusions

Here we have provided a new theoretical framework for the inclusion of horizontal density variations (HDVs) in large-scale ice sheet models, within the shallow ice stream approximation (SSA), and given specific examples of the resulting impact on ice flow. We analysed all previously published approaches to this problem that we could find in the glaciological literature, and provided further new formulations which offer a more complete description of the impact of HDVs on ice flow.

There are several different approaches to including HDVs, some of which require modifications to the typical form of the SSA momentum and mass conservation equa-

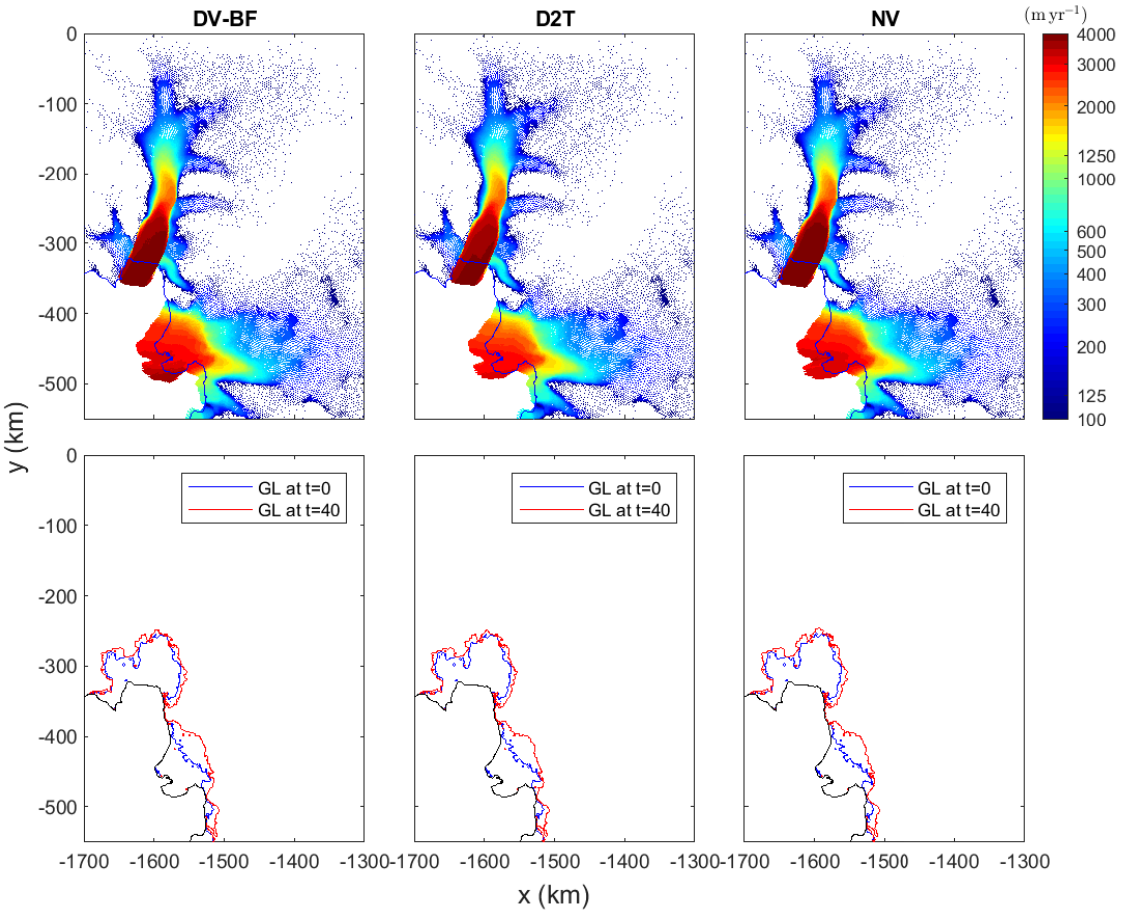

Figure 9. The model velocities (upper panel) and change in grounding line position (lower panel) for the model domain in the Western Antarctic at the end of the simulation after $t = 40$yrs, for each of the density formulations we consider here.

tions. The arguably simplest approach, which requires no modifications to the SSA equations as usually listed in the literature, is to adjust the ice thickness instead of the density. We refer to this commonly-used approach as the *density-to-thickness adjustment* [D2T] throughout this paper. We have shown how this approach leads to the resulting adjustment in ice thickness being advected with the ice, which in effect is equivalent to the initial density variations moving with the ice flow. In a situation where the density and firn thickness distributions are primarily related to atmospheric processes, this might not be very realistic. The key practical advantage of the D2T approach is that it requires no modifications to the typical form of the SSA equations used in large-scale ice-sheet modelling, and only some modifications to the input fields.

An alternative approach to including HDVs in large scale ice-sheet models is to account for them in the body-force term of the momentum-conservation equation, and to express the mass-conservation equation in terms of the product of density and velocity which then implicitly includes variation in the density field. This is referred to as the *Density Variations - Body Force only* [DV-BF] approach in this paper. It requires some modifications to the standard form of the SSA equations, such as including the gradient of density in the body-force term of the momentum equation, as shown in Equation (1). In contrast to the D2T approach, the HDVs are static and do not advect with the ice over time.

We have also suggested two other, arguably more complete, descriptions for including HDVs in ice-flow models, and have shown how these lead to further additional terms in the SSA equations. One is a full implementation of static density variations within the SSA equations, referred to as the DV formulation in this paper. The other is an evolving model, where the initial density distribution advects with the ice, referred to as the DVA formulation in this paper. These two models are both complete descriptions of horizontal density variations, and do not make any approximations about the dominance of certain terms in the SSA equations. The two models span the range of behaviour we might expect for the density evolution. In the DV formulation, the HDVs are static, with the rate of snow accumulation and compactification balanced by the advection of the ice. Based on the observations of Sorge's law (Thomas, 1973) we expect this to be the more realistic formulation. At the other extreme, in the DVA formulation, the atmospheric processes are limited such that density variations are fully advected with the ice flow. To our knowledge, these new options have never been described before and are not implemented in any ice-sheet models to date.

By solving the first-order perturbation analysis in all these various formulations for the inclusion of HDVs, we have provided new insights into the impact of HDVs on large-scale ice flow. We find that the different formulations result in both qualitative and quantitative differences, and they sometimes result in what at first seem somewhat surprising impacts on the ice flow. For example, over floating ice shelves in the D2T approach, density variations lead to an adjustment in the position of the upper surface, while the lower surface elevation is not impacted. The transfer characteristics for the different formulations are qualitatively rather different, as we saw in Figures 2 and 3. The steady-state D2T transfer function is independent of wavelength in all cases, which is only something we observe elsewhere in the explicitly advecting density formulation (DVA) applied to a floating ice shelf. In all the other approaches, the transfer amplitudes depend on the wavelength of the applied density perturbation.

Based on our perturbation analysis, we conclude that the commonly-used D2T approach has very different characteristics to the physically motivated DV formulation. We instead recommend always including the gradient of the density in the body-force term of the momentum equation, and in the mass-conservation equation. This follows what we term the DV-BF approach, and is a closer approximation to the DV formulation. Doing so should only require relatively simple modifications to existing computational models, and have minimal impact on code performance. It is more realistic than the commonly-

used D2T approach, in which all terms involving ice thickness in the SSA equations and boundary conditions are modified by the HDVs, for which there appears to be limited justification.

Finally, we have conducted a numerical study of the West Antarctic Ice Sheet, and provided a specific example of the impact of HDVs on ice flow within the D2T and the DF-BF formulations. We find that HDVs can lead to significant differences in the estimated ice loss over time, although these differences are likely to be small compared to those resulting from uncertainties in the external forcings applied to the model. In our particular simulation (see Figure 8) we find that the resulting difference in projections of global sea level rise is of the order of a few mm over 40 years. While this is, at least in this particular case, not a particularly large difference compared to the overall estimated contribution from WAIS, this result shows that HDVs do impact ice flow and therefore should be taken into account accurately where possible.

Throughout this analysis we have treated the density as constant in the vertical direction, and equal to the vertically-averaged density. This is a necessary assumption in the derivation of the SSA equations in closed form with an arbitrary vertical density profile, and is the first step in correctly incorporating HDVs into vertically-integrated ice sheet models. However, there is scope for further improvement by implementing a parameterised model for the vertical firn distribution. We discuss the implications of this in Appendix B. Extending the vertically-integrated ice sheet models in this way would benefit from coupling to an atmospheric model that predicts the firn density and depth at the surface of the ice sheet.

In this study, we have been concerned with how best to incorporate HDVs into the ice-flow dynamics of vertically-integrated ice-sheet models. This treats the initial vertically-averaged density as an input field to the ice-sheet model, similar to other input fields like the ice sheet bedrock topography or surface mass balance. In reality, we could expect the horizontal density distribution to change over time in response to climate forcings, with different regions experiencing higher or lower snowfall. To incorporate the changes due to climate forcings would require coupling to an atmospheric model which has a complete description of the surface processes (such as surface melt, refreezing, firn accumulation) that lead to HDVs in the ice sheet. This would allow the horizontal density distribution to be updated inside the ice sheet model as it evolves.

Appendix A Vertical Integration of the Field Equations

In this appendix, we derive the modified SSA field equations that were presented in section 2 which take into account horizontal variation in glacial density. These equations appear to have been derived for the first time by Morland (1987), although then intended to describe the flow of ice shelves only. Subsequently they were derived for coupled ice-shelf/ice-stream flow by Muszynski and Birchfield (1987), and then for grounded ice where most of the motion is due to sliding by MacAyeal (1989). They have been derived numerous times in various papers since then, e.g. (Baral et al., 2001; Schoof, 2006), and well-summarised in the review article by Schoof and Hewitt (2013). Here we broadly followed the derivation given in Gudmundsson (2020a), but with various modifications and extensions to account for a variable density field.

We start by defining the vertically-integrated density:

$$\langle \rho \rangle = \frac{1}{h} \int_b^s \rho(z)\, \mathrm{d}z$$

where h is the ice-sheet thickness, and s and b are the upper and lower ice surface elevations, respectively. This expression can be split into a meteoric ice layer of density

ρ_{ice}, and a firn layer of thickness F and variable density ρ_{firn}:

$$\langle\rho\rangle = \frac{1}{h}\left(\int_b^{s-F} \rho_{\text{ice}}\,\mathrm{d}z + \int_{s-F}^{s} \rho_{\text{firn}}(z)\,\mathrm{d}z\right)$$

From this we can define the *firn air-content*:

$$\delta \equiv \int_{s-F}^{s} \frac{\rho_{\text{ice}} - \rho_{\text{firn}}(z)}{\rho_{\text{ice}}}\mathrm{d}z$$

which represents the vertical distance by which the firn needs to be compacted for it to have acquired the same density as that of ice, such that

$$\langle\rho\rangle = \rho_{\text{ice}}\,(1 - \delta/h)$$

and

$$\rho_{\text{ice}} \times h_{\text{ice}} = \langle\rho\rangle \times h$$

where $h_{\text{ice}} \equiv h - \delta$ is the ice-equivalent thickness. In all that follows, we make the simplifying assumption that the density is constant with depth and equal to the vertically averaged density, i.e. that at each spatial point the density $\rho(x, y, z)$ is given by the vertically averaged density $\langle\rho\rangle(x, y)$. Without this assumption, analytical solutions to the vertically-integrated field equations are not possible, and would instead require numerical integration and differentiation in the z-dimension, which is incompatible with shallow-ice models. In all that follows we assume that the glacial density $\rho(x, y, z) = \rho(x, y)$ and we drop the angle brackets to indicate the vertical average.

A1 Momentum Equations

The shallow-ice stream approximation (SSA) applies to ice flows where the depth of the ice sheet is much smaller than the horizontal dimensions. See MacAyeal (1989) for a detailed discussion of the approximation. Within this approximation, the momentum-conservation equations describing the ice flow in a tilted coordinate system that is parallel to the bed topography are

$$\partial_x\sigma_{xx} + \partial_y\tau_{xy} + \partial_z\tau_{xz} = -\rho g \sin\alpha \tag{A1}$$

$$\partial_x\tau_{xy} + \partial_y\sigma_{yy} + \partial_z\tau_{yz} = 0 \tag{A2}$$

$$\partial_z\sigma_{zz} = \rho g \cos\alpha \tag{A3}$$

where α is the angle of the coordinate system to the horizontal, and σ_{ij} and τ_{ij} are the Cauchy and deviatoric stress components respectively. The Cauchy and deviatoric stresses are related through the pressure: $\tau_{ij} = \delta_{ij}p + \sigma_{ij}$. The deviatoric stresses are related to the strain rates through the effective viscosity:

$$\tau_{ij} \equiv 2\eta\dot{\epsilon}_{ij}$$

with the strain rate given by

$$\dot{\epsilon}_{ij} \equiv \frac{1}{2}\left(\partial_i v_j + \partial_j v_i\right)$$

The viscosity is often described by a model such as Glen's flow law:

$$\dot{\epsilon}_{ij} = A\tau^{n-1}\tau_{ij} \tag{A4}$$

with rate factor A and exponent n. In some ice-flow models, the rate factor describing the ice rheology is allowed to vary with depth since it is strongly dependent on temperature, and treated as a vertically-integrated quantity. However in this derivation, we assume the rate factor A is constant with depth, and consequently that the effective viscosity η is constant with depth in the SSA. In the SSA, the horizontal velocities are independent of depth, and the vertical velocity varies linearly with depth. Thus by definition τ_{xx}, τ_{xy} and τ_{yy} are also independent of z.

To find the vertically integrated solution to these equations, we need to impose the boundary conditions at the upper surface:

$$\begin{aligned} -\sigma_{xx}\partial_x s - \tau_{xy}\partial_y s + \tau_{xz} &= 0 \\ -\sigma_{yy}\partial_y s - \tau_{xy}\partial_x s + \tau_{yz} &= 0 \\ \sigma_{zz} &= 0 \end{aligned}$$

together with the boundary conditions at the lower surface:

$$\begin{aligned} t_{bx} &= (\sigma_{zz} - \sigma_{xx})\partial_x b - \tau_{xy}\partial_y b + \tau_{xz} \\ t_{by} &= (\sigma_{zz} - \sigma_{yy})\partial_y b - \tau_{xy}\partial_x b + \tau_{yz} \end{aligned}$$

where t_{bx} and t_{by} are the horizontal components of the basal traction vector. We start by integrating Equation (A3) from z to $z = s(x, y)$:

$$\sigma_{zz}(s) - \sigma_{zz}(z) = (s - z)\,\rho g \cos\alpha$$

The boundary conditions at the surface impose $\sigma_{zz}(s) = 0$ and so

$$\sigma_{zz}(z) = -\,(s - z)\,\rho g \cos\alpha \tag{A5}$$

Integrating again, we arrive at

$$\partial_x \int_b^s \sigma_{zz}(z)\mathrm{d}z = \sigma_{zz}(b)\partial_x h - \frac{1}{2}h^2\partial_x \rho g \cos\alpha \tag{A6}$$

The next step is to integrate Equation (A1) from $z = b(x, y)$ to $z = s(x, y)$:

$$\int_b^s \partial_x \sigma_{xx}\mathrm{d}z + \int_b^s \partial_y \tau_{xy}\mathrm{d}z + \int_b^s \partial_z \tau_{xz}\mathrm{d}z = -\rho g h \sin\alpha$$

and use Leibniz' rule to interchange the order of integration and differentiation:

$$\begin{aligned} &\partial_x \int_b^s \sigma_{xx}\mathrm{d}z - \sigma_{xx}(s)\partial_x s + \sigma_{xx}(b)\partial_x b \\ &+\partial_y \int_b^s \tau_{xy}\mathrm{d}z - \tau_{xy}(s)\partial_x s + \tau_{xy}(b)\partial_x b \\ &\qquad +\tau_{xz}(s) - \tau_{xz}(b) = -\rho g h \sin\alpha \end{aligned}$$

Substituting the boundary conditions at the upper and lower surface, we arrive at

$$\partial_x \int_b^s \sigma_{xx}\mathrm{d}z + \sigma_{zz}(b)\partial_x b - t_{bx} + \partial_y \int_b^s \tau_{xy}\mathrm{d}z = -\rho g h \sin\alpha \tag{A7}$$

The next step of the derivation is to express σ_{xx} in terms of σ_{zz} and other quantities which are independent of z. Based on the definition of the deviatoric stresses, we can write

$$\sigma_{xx} = \tau_{xx} - \tau_{zz} + \sigma_{zz} \tag{A8}$$

and eliminate τ_{zz} (which varies with depth) by using the mass-conservation equation as follows. The generalised form of the mass-conservation equation is given by Equation (2). In the typical derivation for the vertical-integration of the momentum equations in the SSA, the density is assumed constant and the constraint simplifies to $\boldsymbol{\nabla}\cdot\boldsymbol{v}$. However, if we use the mass conservation equation for compressible material (Equation (2)), and substitute the expression for the deviatoric stresses in terms of the velocity gradients, then we arrive at

$$-\tau_{zz} = \tau_{xx} + \tau_{yy} + \frac{2\eta}{\rho}\frac{D\rho}{Dt} \tag{A9}$$

The additional term, which scales as the material derivative of ρ, does not appear if we assume a constant density ice sheet. It also disappears if we assume that the initial density distribution advects with the ice, such that $D\rho/Dt = 0$. Substituting Equation (A9) into Equation (A8), we arrive at

$$\sigma_{xx} = \sigma_{zz} + 2\tau_{xx} + \tau_{yy} + \frac{2\eta}{\rho}\frac{D\rho}{Dt} \tag{A10}$$

where all terms on the right hand side of the equation apart from σ_{zz} are independent of depth in the SSA. Substituting Equation (A10) into Equation (A7), we find

$$\partial_x \int_b^s \sigma_{zz} \mathrm{d}z + \partial_x \left(2h\tau_{xx} + h\tau_{yy} + \frac{2\eta h}{\rho}\frac{D\rho}{Dt}\right) + \sigma_{zz}(b)\partial_x b - t_{bx} + \partial_y(h\tau_{xy}) = -\rho g h \sin\alpha \tag{A11}$$

Inserting Equation (A6) into Equation (A11), we arrive at the first vertically-integrated momentum equation:

$$\partial_x \left(2h\tau_{xx} + h\tau_{yy} + \frac{2\eta h}{\rho}\frac{D\rho}{Dt}\right) + \partial_y(h\tau_{xy}) - t_{bx} = \rho g h \left(\partial_x s \cos\alpha - \sin\alpha\right) + \frac{1}{2}h^2 g \partial_x \rho \cos\alpha \tag{A12}$$

The procedure can be repeated for Equation (A2), where we use the relationship,

$$\sigma_{yy} = \sigma_{zz} + 2\tau_{yy} + \tau_{xx} + \frac{2\eta}{\rho}\frac{D\rho}{Dt}$$

to derive the second vertically-integrated momentum equation:

$$\partial_y \left(2h\tau_{yy} + h\tau_{xx} + \frac{2\eta h}{\rho}\frac{D\rho}{Dt}\right) + \partial_x(h\tau_{xy}) - t_{by} = \rho g h \partial_y s \cos\alpha + \frac{1}{2}h^2 g \partial_y \rho \cos\alpha$$

These results can be expressed in terms of the components of the velocity vector:

$$\begin{aligned}
&\partial_x \left(4h\eta\partial_x u + 2h\eta\partial_y v + \frac{2h\eta}{\rho}\frac{D\rho}{Dt}\right) \\
&\qquad + \partial_y(h\eta(\partial_x v + \partial_y u)) - t_{bx} = \rho g h \left(\partial_x s \cos\alpha - \sin\alpha\right) + \frac{1}{2}h^2 g \partial_x \rho \cos\alpha \\
&\partial_y \left(4h\eta\partial_y v + 2h\eta\partial_x u + \frac{2h\eta}{\rho}\frac{D\rho}{Dt}\right) \\
&\qquad + \partial_x(h\eta(\partial_x v + \partial_y u)) - t_{by} = \rho g h \partial_y s \cos\alpha + \frac{1}{2}h^2 g \partial_y \rho \cos\alpha
\end{aligned}$$

where u and v are the horizontal velocities in the x and y direction respectively.

A2 Mass-Conservation Equation

The generalised form of the mass-conservation equation which allows for density variation in the ice sheet is

$$\boldsymbol{\nabla} \cdot (\rho \boldsymbol{v}) + \partial_t \rho = 0 \tag{A13}$$

To solve the vertical integration of this equation, we require the kinematic boundary conditions:

$$\begin{aligned}
\partial_t s + u\partial_x s + v\partial_x s - w_s &= a_s \\
\partial_t b + u\partial_x b + v\partial_x b - w_b &= -a_b
\end{aligned} \tag{A14}$$

where the horizontal velocities are independent of depth in the SSA; w_s, w_b are the vertical velocity components at the upper and lower surfaces respectively; and a_s and a_b are the surface accumulation rate and basal melt rates respectively. Integrating Equation (A13) from $z = b(x, y)$ to $s(x, y)$:

$$\int_b^s \left(\partial_x(\rho u) + \partial_y(\rho v) + \partial_z(\rho w)\right) \mathrm{d}z + h\partial_t \rho = 0$$

Changing the order of differentiation using Leibniz rule:

$$\boldsymbol{\nabla}_{xy} \cdot \boldsymbol{q}_{xy} - \rho u \partial_x h - \rho v \partial_y h + \rho(w_s - w_b) + h\partial_t \rho = 0$$

where ρ is assumed constant with depth, and we have introduced the horizontal mass flux which is defined as

$$\boldsymbol{q}_{xy} \equiv \int_b^s \rho \boldsymbol{v}_{xy} \, \mathrm{d}z$$

Substituting Equations (A14), we arrive at the vertically integrated mass-conservation equation:

$$\rho \partial_t h + \boldsymbol{\nabla}_{xy} \cdot \boldsymbol{q}_{xy} + h\partial_t \rho = \rho a$$

where the total accumulation $a = a_s + a_b$.

A3 Boundary Conditions at the Calving Front

The variation in the density distribution also has an impact on the boundary conditions that exist at the calving front, a key constraint applied in shallow-ice models. At the calving front Γ_c, we require balance of the vertically-integrated horizontal stresses. In the x and y directions, this stress condition is

$$\begin{aligned} \int_b^s (\sigma_{xx} n_x + \tau_{xy} n_y) \, \mathrm{d}z &= -\int_b^S p_w n_x \mathrm{d}z \\ \int_b^s (\tau_{xy} n_x + \sigma_{yy} n_y) \, \mathrm{d}z &= -\int_b^S p_w n_y \mathrm{d}z \end{aligned} \tag{A15}$$

where p_w is the hydrostatic ocean pressure, n_x and n_y are the components of the unit normal pointing horizontally outward from the ice front, and S is the surface of the ocean. The x-component of the vertically-integrated ocean pressure acting on the calving front, can be solved to give

$$-\int_b^S p_w n_x \mathrm{d}z = -\frac{1}{2}\rho_w g d^2 n_x \tag{A16}$$

where $d \equiv S - b$ is the draft at the ice front. Meanwhile, combining Equations (A10) and (A5), we have

$$\sigma_{xx} = -(s - z)\rho g + 2\tau_{xx} + \tau_{yy} + \frac{2\eta}{\rho}\frac{D\rho}{Dt}$$

where $\alpha = 0$ in this coordinate system. Integrating from $z = b$ to s:

$$\int_b^s \sigma_{xx} \mathrm{d}z = h\left(2\tau_{xx} + \tau_{yy} + \frac{2\eta}{\rho}\frac{D\rho}{Dt}\right) - \frac{1}{2}\rho g h^2 \tag{A17}$$

Substituting Equations (A16) and (A17) into Equation (A15), we arrive at the boundary conditions at the calving front:

$$\begin{aligned} h\left(2\tau_{xx} + \tau_{yy} + \frac{2\eta}{\rho}\frac{D\rho}{Dt}\right) n_x + h\tau_{xy} n_y &= \frac{1}{2} g \left(\rho h^2 - \rho_w d^2\right) n_x \\ h\left(2\tau_{yy} + \tau_{xx} + \frac{2\eta}{\rho}\frac{D\rho}{Dt}\right) n_y + h\tau_{xy} n_x &= \frac{1}{2} g \left(\rho h^2 - \rho_w d^2\right) n_y \end{aligned}$$

which can alternatively be expressed in terms of the velocity components as

$$\begin{aligned} 2\eta h\left(2\partial_x u + \partial_y v + \frac{1}{\rho}\frac{D\rho}{Dt}\right) n_x + \eta h \left(\partial_x v + \partial_y u\right) n_y &= \frac{1}{2} g \left(\rho h^2 - \rho_w d^2\right) n_x \\ 2\eta h\left(2\partial_y v + \partial_x u + \frac{1}{\rho}\frac{D\rho}{Dt}\right) n_y + \eta h \left(\partial_x v + \partial_y u\right) n_x &= \frac{1}{2} g \left(\rho h^2 - \rho_w d^2\right) n_y \end{aligned}$$

A4 Effective Viscosity

Variations in the density field can also have an impact on the derivation of the effective viscosity in shallow-ice models. A simple linear model for viscosity, such that η is a constant, will be unaffected. However in general, the rheology of the ice can be described by a model such as Glen's flow law in Equation (A4), for which the effective viscosity is

$$\eta = \frac{1}{2} A^{-1/n} \dot{\epsilon}^{(1-n)/n}$$

where $\dot{\epsilon} = \sqrt{\dot{\epsilon}_{ij}\dot{\epsilon}_{ij}/2}$ is the *effective strain rate*. In the SSA, the components $\dot{\epsilon}_{xz}$ and $\dot{\epsilon}_{yz}$ are second order and can be neglected. Thus,

$$\dot{\epsilon} = \sqrt{(\dot{\epsilon}_{xx}^2 + \dot{\epsilon}_{yy}^2 + \dot{\epsilon}_{zz}^2)/2 + \dot{\epsilon}_{xy}^2}$$

In the vertically-integrated approach, $\dot{\epsilon}_{zz}$ is unknown and specified via the mass-conservation:

$$\dot{\epsilon}_{ii} = \boldsymbol{\nabla} \cdot \boldsymbol{v} = -\frac{1}{\rho}\frac{D\rho}{Dt}$$

which leads to

$$\dot{\epsilon}_{zz}^2 = \left(\dot{\epsilon}_{xx} + \dot{\epsilon}_{yy} + \frac{1}{\rho}\frac{D\rho}{Dt}\right)^2$$

Appendix B Vertically-Varying Density Profile

In the preceding derivation of the SSA equations, we assumed that the density of the ice sheet was constant with depth and equal to the vertically-averaged density, because it is not possible to derive the SSA equations in a closed form for an arbitrary vertical density profile. In this appendix, we explore this decision in a bit more detail.

In Thomas (1973) there is a discussion of the impact of vertical variations in density on the creep of ice shelves. They found that the effective shear stress at the ice-shelf front was overestimated by a factor of two if the density was treated as constant, compared to assuming a particular (exponential) form for the vertical density profile. However, this relationship is determined by the value of the double integral $\int_b^s \int_z^s \rho(z')\mathrm{d}z'\mathrm{d}z$ relative to the hydrostatic pressure at the ice front, and is not indicative of the effects we could expect to see in the SSA equations, where it is the horizontal gradient of the double integral that is the driving force.

The key step in the derivation of the SSA equations occurs at Equations (A5) and (A6), where the density field is integrated twice with respect to z. If we allowed for a depth-varying density field, then equation A6 instead becomes:

$$\partial_x \int_b^s \sigma_{zz}(z)\mathrm{d}z = -\partial_x \left(\int_b^s \int_z^s \rho(z')\mathrm{d}z'\mathrm{d}z\right) g\cos\alpha \tag{B1}$$

This integral cannot be further evaluated without specifying the form of the vertical density profile. The simplest assumption is that the density is constant with depth. This is what we have done in the derivation of the SSA field equations and underpins the results presented in this paper. We could instead consider some parameterisations of the vertical density profile which we explore further below.

One formulation is to model the density as two distinct layers: the bottom layer is pure ice with density ρ_{ice}; the top layer is firn with constant density $\rho_{\mathrm{firn}} = 500\mathrm{kg/m}^3$. The thickness of the firn layer varies to match the measurements of the vertically averaged density. With this model for the vertical density profile, we can solve the double integral:

$$\int_b^s \int_z^s \rho(z')\mathrm{d}z'\mathrm{d}z = \frac{1}{2}\bar{\rho}h(h-h_f) + \frac{1}{2}\rho_{\mathrm{firn}}h_f h \tag{B2}$$

where h_f is the thickness of the firn layer, and by definition

$$\bar{\rho} \times h = \rho_{\text{ice}}(h - h_f) + \rho_{\text{firn}} h_f$$

With this model for the vertical density profile, Equation (A6) becomes

$$\partial_x \int_b^s \sigma_{zz}(z)\mathrm{d}z = \sigma_{zz}(b)\partial_x h - ((h - h_f)h\partial_x\bar{\rho} - (\bar{\rho} - \rho_{\text{firn}})h_f\partial_x h)\, g\cos\alpha \tag{B3}$$

This propagates through the derivation, and modifies the driving force on the right-hand side of the SSA momentum Equation (A12). It becomes

$$\tau_{\text{driving}}^{\text{2-layer}} = \bar{\rho}gh\,(\partial_x s\cos\alpha - \sin\alpha) + ((h - h_f)h\partial_x\bar{\rho} - (\bar{\rho} - \rho_{\text{firn}})h_f\partial_x h)\, g\cos\alpha \tag{B4}$$

Previously, when assuming a constant vertical density profile, the driving force was

$$\tau_{\text{driving}}^{\text{constant}} = \bar{\rho}gh\,(\partial_x s\cos\alpha - \sin\alpha) + \frac{1}{2}h^2 g\partial_x\rho\cos\alpha \tag{B5}$$

In the D2T adjustment, the firn layer is effectively modeled as $h_f = \delta$ (the firn correction) and $\rho_{\text{firn}} = 0$. Substituting these values into Equation (B4), this does indeed recover the RHS of the momentum equation presented in Equation (26):

$$\tau_{\text{driving}}^{\text{D2T}} = \bar{\rho}gh\,(\partial_x s\cos\alpha - \sin\alpha) + ((h - \delta)h\partial_x\bar{\rho} - \bar{\rho}\delta\partial_x h)\, g\cos\alpha \tag{B6}$$

It should be noted that in the D2T formulation, terms on the left-hand side of the momentum equation multiplying the viscosity are also modified, as demonstrated in section 5.5.

An alternative formulation is to model the density with the exponential vertical profile described in Thomas (1973):

$$\rho(z) = \rho_{\text{ice}} - (\rho_{\text{ice}} - \rho_{\text{firn}})e^{-\nu(s-z)}$$

where ρ_{firn} is the density at the surface, and ν is the decay parameter. Typically $\nu \sim 5/h$. If we fix the density at the surface, we have a one-to-one relationship between the decay parameter and the vertically-averaged density:

$$\nu^{-1} = \left(\frac{\rho_{\text{ice}} - \bar{\rho}}{\rho_{\text{ice}} - \rho_{\text{firn}}}\right) h$$

Following through the derivation, the driving force on the right-hand side of the SSA momentum Equation (A12) in this case becomes

$$\tau_{\text{driving}}^{\text{exponential}} = \bar{\rho}gh\,(\partial_x s\cos\alpha - \sin\alpha) + \left(h - \frac{2}{\nu}\right)(h\partial_x\bar{\rho} - (\rho_{\text{ice}} - \bar{\rho})\partial_x h)\, g\cos\alpha \tag{B7}$$

where the exponential term is dropped once the double integral has been performed because $e^{-\nu h} \ll 1$.

Substituting some typical values into the different expressions for the driving force in Equations (B4, B5, B6 & B7), we find that the correction due to HDVs consists of a term proportional to $h^2\partial_x\rho$ with a coefficient that ranges from 0.5 (constant vertical density) to 0.9 (D2T approximation) and another much smaller correction term that is proportional to $h\partial_x h$. The assumption of constant vertical density is a good first approximation, but this highlights that the HDV correction term in the SSA equations is sensitive to the exact parameterisation of the vertical density profile that is assumed. This is a limitation inherent in any vertically-integrated ice-sheet model. For a more comprehensive treatment it would be necessary to resort to a 3-D ice sheet model.

Appendix C The Equilibrium Profile for a Floating Ice-Shelf

Starting from the momentum conservation in Equation (32), we derive the equilibrium profile for a floating ice-shelf. This is a well-known solution in glaciology, with one of the earliest derivations, to our knowledge, being that in Van der Veen (1983). Setting the density of the ice shelf to be constant, we also assume linear viscosity such that $\eta = \text{const}$, and constant surface mass-balance, $a = a_s + a_b$. It is important that $a \neq 0$, otherwise this is not a steady-state solution, and instead the ice shelf spreads out infinitely thinly. The momentum-conservation simplifies to

$$\partial_x u = \frac{\varrho g h}{8\eta} \tag{C1}$$

and in a steady-state, with constant density, the vertically-integrated mass-conservation in Equation (3) reduces to

$$\partial_x (uh) = a \tag{C2}$$

Integrating this equation, and setting $x = 0$ at the grounding line (or some arbitrary point on the ice shelf) without loss of generality, we have

$$u(x)h(x) - q_{\text{gl}} = ax \tag{C3}$$

where $q_{\text{gl}} = u|_{x=0} h|_{x=0}$. Substituting the expressions for $\partial_x u$ and $u(x)$, from Equations (C1) and (C3) respectively, into Equation (C2), we find

$$\frac{\varrho g h^2}{8\eta} + \frac{ax + q_{\text{gl}}}{h} \partial_x h = a$$

which can be rearranged to

$$\left(\frac{h^{-3}}{ah^{-2} - \varrho g / 8\eta} \right) \frac{\mathrm{d}h}{\mathrm{d}x} = \frac{1}{(ax + q_{\text{gl}})}$$

Integrating both sides we arrive at the steady-state solution:

$$h(x) = \left[\frac{1}{a} \left(\frac{K}{(ax + q_{\text{gl}})^2} + \frac{\varrho g}{8\eta} \right) \right]^{-\frac{1}{2}}$$

and

$$u(x) = \left[\frac{1}{a} \left(K + \frac{\varrho g}{8\eta} (ax + q_{\text{gl}})^2 \right) \right]^{\frac{1}{2}}$$

where K is an arbitrary integration constant, which can be determined by specifying the thickness at $x = 0$:

$$K = q_{gl}^2 \left(\frac{a}{h_{gl}^2} - \frac{\varrho g}{8\eta} \right)$$

where $h|_{x=0} = h_{gl}$. We have plotted the equilibrium positions of the velocity, and upper and lower surfaces, of a floating ice shelf in Figure C1.

Appendix D Numerical vs Analytical Perturbations

In Figure D1, we compare the analytical results presented in Figures 4 and 5, to numerical simulations performed in the large-scale ice-flow model Úa, for each of the different approaches to include HDVs: *Density Variations* [DV], *Density Variations - Body Force only* [DV-BF] and *Density-to-Thickness adjustment* [D2T]. To arrive at these results required a modification to Úa to include additional terms in the momentum equation in order to replicate the DV formulation. The DVA formulation, which requires the density distribution to evolve over time in the model, is not implemented in Úa, and so not included here.

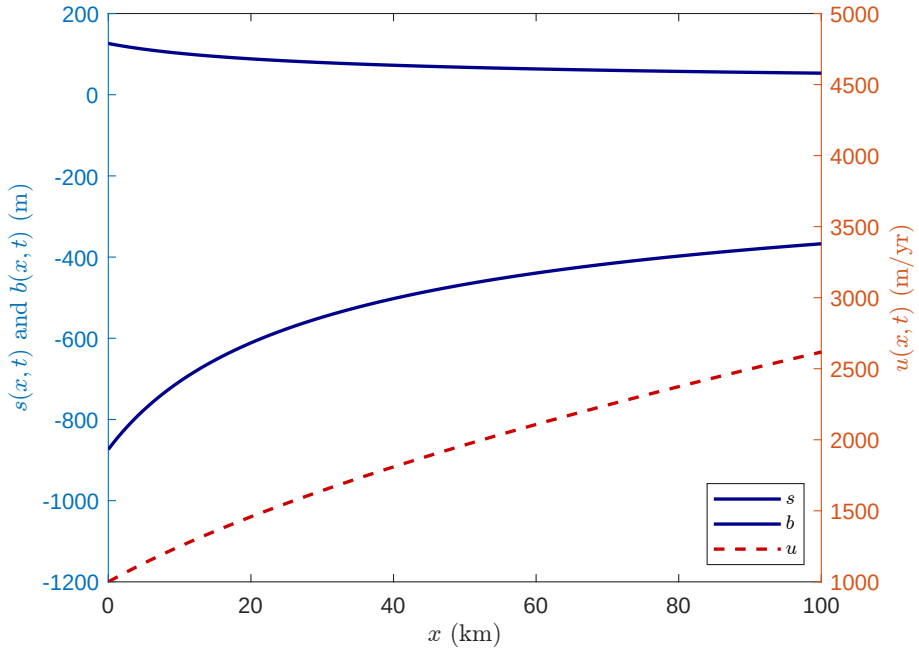

Figure C1. Equilibrium positions of the upper and lower surfaces, $s(x,t)$ and $b(x,t)$ [solid lines], and velocity, $u(x,t)$ [dashed line], for the floating ice shelf. In this example, we set $\bar{\rho} = 900\,\mathrm{kg/m^3}$, $\eta = 5 \times 10^3\,\mathrm{kPa \cdot yr}$ and the surface accumulation $a_s = 1\,\mathrm{m/yr}$.

The numerical and analytical results match very closely, which gives us confidence that no mistakes were made in the analytical derivations, and that Úa is behaving correctly. The close match for the floating ice shelf is important, and confirms the validity of the approximation proposed in Ng et al. (2018), as well as the approach taken to mask the $k = 0$ component of the transfer function to avoid the transfer function (in this approximation) blowing up to infinity.

Notation

$\boldsymbol{\partial_x}$ partial derivative w.r.t. x
$\frac{\boldsymbol{D}}{\boldsymbol{Dt}}$ material derivative
$\boldsymbol{\alpha}$ slope of the basal surface
$\boldsymbol{\beta}$ defined through $\beta \equiv \frac{\bar{\rho} g \bar{h}}{8\eta}$
$\boldsymbol{\gamma}$ defined through $\gamma \equiv \tau_d^{1-m}/mc$
$\boldsymbol{\delta}$ firn air-content of the ice sheet
$\boldsymbol{\dot{\epsilon}_{ij}}$ strain rates
$\boldsymbol{\zeta}$ defined through $\zeta \equiv 2\eta h k^2 \xi^{-1}$
$\boldsymbol{\eta}$ vertically-integrated effective viscosity
$\boldsymbol{\lambda}$ wavelength
$\boldsymbol{\xi}$ defined through $\xi \equiv \gamma + 4hk^2\eta$
$\boldsymbol{\rho}$ vertically-averaged ice-sheet density
$\boldsymbol{\rho_{\mathrm{ice}}}$ density of pure meteoric ice, $917\,\mathrm{kg\,m^{-3}}$
$\boldsymbol{\rho_w}$ density of the ocean, $1030\,\mathrm{kg\,m^{-3}}$
$\boldsymbol{\varrho}$ defined through $\varrho \equiv \rho(1 - \rho/\rho_w)$
$\boldsymbol{\sigma_{ij}}$ components of the Cauchy stress tensor
$\boldsymbol{\tau_{ij}}$ deviatoric stresses

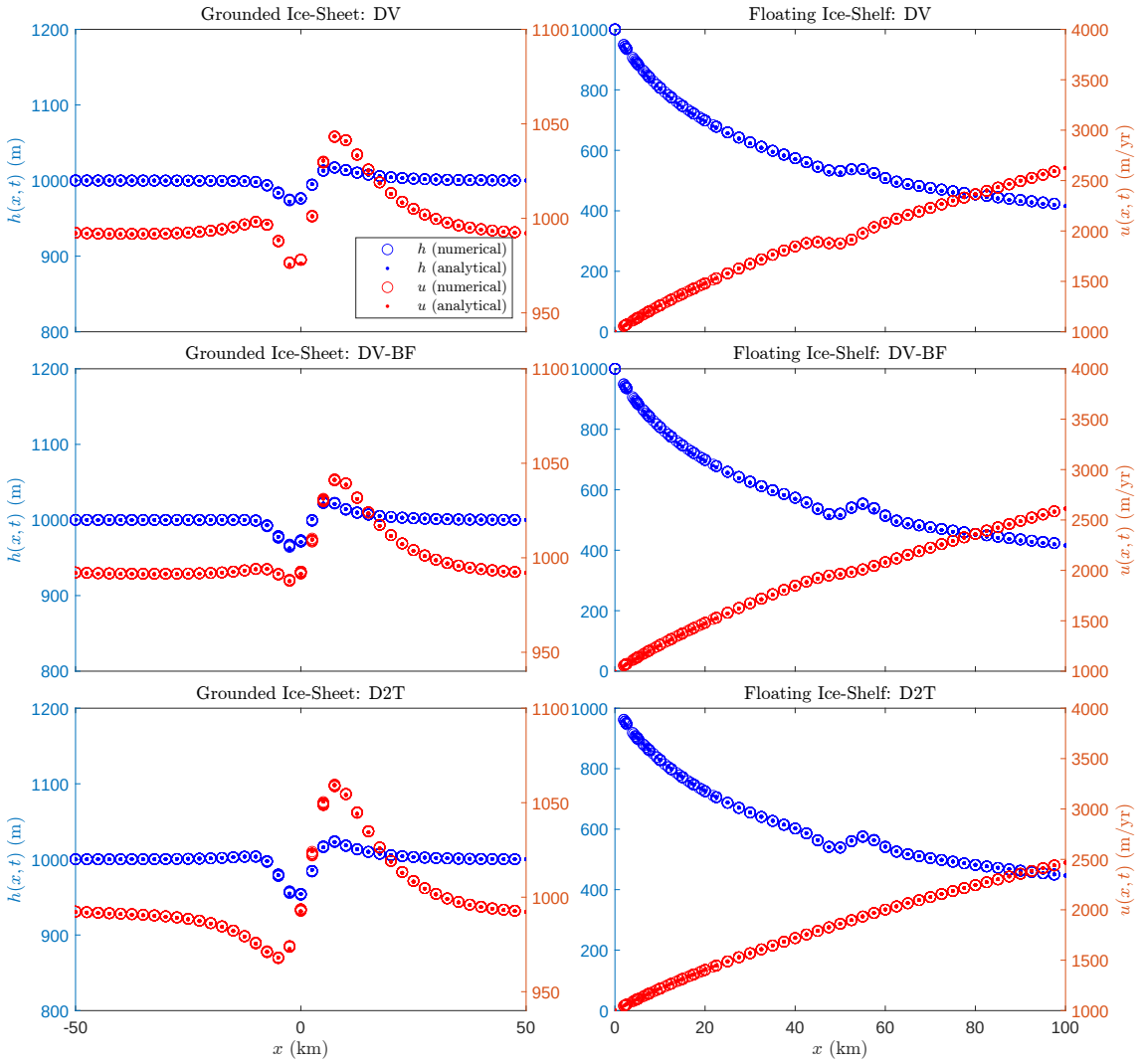

Figure D1. Example of the spatial distribution in $h(x,t)$ and $u(x,t)$ at t = 2yrs after an initial 10% Gaussian density perturbation applied in $\Delta\rho$. This compares the analytical response to a full numerical simulation in Úa. The simulation parameters are the same as those specified in Figures 4 and 5.

$\boldsymbol{\tau_d}$ driving stress
$\boldsymbol{\phi}$ defined through $\phi \equiv 1 - \frac{\partial_x \bar{h}}{ik\bar{h}}$
$\boldsymbol{\phi^\star}$ defined through $\phi^\star \equiv 1 + \frac{\partial_x \bar{h}}{ik\bar{h}}$
$\boldsymbol{\omega}$ angular frequency
$\boldsymbol{a}$ total accumulation, $a_s + a_b$
$\boldsymbol{a_b}$ basal melt
$\boldsymbol{a_s}$ surface accumulation
$\boldsymbol{A}$ rate factor in Glen's flow law
$\boldsymbol{b}$ lower glacial surface
$\boldsymbol{c, C}$ basal slipperiness
$\boldsymbol{d}$ draft at the ice-front: $S - b$
$\boldsymbol{h}$ total glacial thickness
$\boldsymbol{h_{\mathbf{ice}}}$ ice-equivalent thickness, $h - \delta$
$\boldsymbol{\mathcal{H}(t)}$ Heaviside step function
$\boldsymbol{k}$ wavenumber in the x-direction
$\boldsymbol{m}$ exponent in Weertman's sliding law
$\boldsymbol{n_i}$ components of unit normal vector
$\boldsymbol{p}$ pole in the Laplace frame for the grounded ice perturbations, $it_p^{-1} - t_r^{-1}$
$\boldsymbol{p_{\mathbf{FL}}}$ pole in the Laplace frame for the floating ice perturbations, $iku - \phi\partial_x u$
$\boldsymbol{q_{xy}}$ horizontal mass-flux
$\boldsymbol{r}$ laplace transform variable
$\boldsymbol{s}$ upper glacial surface
$\boldsymbol{S}$ ocean surface
$\boldsymbol{t}$ time
$\boldsymbol{t_b = (t_{bx}, t_{by})}$ basal drag
$\boldsymbol{t_p}$ phase timescale
$\boldsymbol{t_r}$ relaxation timescale
$\boldsymbol{v, \{v_i\}, (u, v, w)}$ components of the velocity vector
$\boldsymbol{v_b}$ basal velocity

Acknowledgments

This work was supported and carried out as a part of the NSFGEO-NERC funded project *Processes, drivers, predictions: Modelling the response of Thwaites Glacier over the next century using ice/ocean coupled models* (NE/S006745/1).

Availability Statement

All numerical simulations in this study were performed with the shallow-ice model Úa. The source code of Úa can be downloaded from https://github.com/GHilmarG/UaSource (Gudmundsson, 2020b). The input and output files for the experiments presented in this paper, as well as the MATLAB code for computing the transfer functions, can be accessed at https://doi.org/10.5281/zenodo.6501217. For the numerical simulations of the Western Antarctic Ice Sheet: the geometry inputs are from BedMachine Antarctica v.2 (Morlighem, 2020; Morlighem et al., 2020) which can be downloaded from https://doi.org/10.5067/E1QL9HFQ7A8M; the surface mass balance inputs derive from RACMO v2.3 (Van Wessem et al., 2014) which can be accessed via https://www.projects.science.uu.nl/iceclimate/models/racmo-archive.php; and the surface velocity data was generated using auto-RIFT (Gardner, Moholdt, et al., 2018) and provided by the NASA MEaSUREs ITS_LIVE project (Gardner, Fahnestock, & Scambos, 2018), which can be accessed at https://doi.org/10.5067/IMR9D3PEI28U.

References

Bader, H. (1954). Sorges law of densification of snow on high polar glaciers. *Journal of Glaciology*, *2*, 319-323. doi: 10.3189/S0022143000025144

Baral, D. R., Hutter, K., & Greve, R. (2001). Asymptotic theories of large-scale motion, temperature, and moisture distribution in land-based polythermal ice sheets: A critical review and new developments. *Applied Mechanics Reviews*, *54*, 215256. doi: 10.1115/1.3097296

Barnes, J. M., dos Santos, T. D., Goldberg, D., Gudmundsson, G. H., Morlighem, M., & Rydt, J. D. (2021). The transferability of adjoint inversion products between different ice flow models. *The Cryosphere*, *15*, 1975-2000. doi: 10.5194/tc-15-1975-2021

Bueler, E., & Brown, J. (2009). Shallow shelf approximation as a "sliding law" in a thermodynamically coupled ice sheet model. *J. Geophys. Res.*, *114*, F03008. doi: 10.1029/2008JF001179

Cornford, S. L., Martin, D. F., Graves, D. T., Ranken, D. F., Le Brocq, A. M., Gladstone, R. M., ... Lipscomb, W. H. (2013). Adaptive mesh, finite volume modeling of marine ice sheets. *Journal of Computational Physics*, *232*, 529-549.

De Rydt, J., Reese, R., Paolo, F. S., & Gudmundsson, G. H. (2021). Drivers of pine island glacier speed-up between 1996 and 2016. *The Cryosphere*, *15*, 113-132. doi: 10.5194/tc-15-113-2021

Gardner, A. S., Fahnestock, M. A., & Scambos, T. A. (2018). Measures its_live landsat image-pair glacier and ice sheet surface velocities: Version 1. doi: 10.5067/IMR9D3PEI28U

Gardner, A. S., Moholdt, G., Scambos, T., Fahnstock, M., Ligtenberg, S., Van Den Broeke, M., & Nilsson, J. (2018). Increased west antarctic and unchanged east antarctic ice discharge over the last 7 years. *The Cryosphere*, *12*, 521547. doi: 10.5194/tc125212018

Gudmundsson, G. H. (2008). Analytical solutions for the surface response to small amplitude perturbations in boundary data in the shallow-ice-stream approximation. *The Cryosphere*, *2*, 77-93. doi: 10.5194/tc-2-77-2008

Gudmundsson, G. H. (2020a). Úa compendium. Retrieved from `https://github.com/GHilmarG/UaSource/blob/master/UaCompendium.pdf` (date accessed: Oct 2021)

Gudmundsson, G. H. (2020b). Úa (v2019b). Retrieved from `https://github.com/GHilmarG/UaSource` (date accessed: Oct 2021) doi: 10.5281/zenodo.3706624

Hoffman, M. J., Perego, M., Price, S. F., Lipscomb, W. H., Zhang, T., Jacobsen, D., ... Bertagna, L. (2018). Mpas-albany land ice (mali): a variable-resolution ice sheet model for earth system modeling using voronoi grids. *Geosci. Model Dev.*, *11*, 3747-3780. doi: 10.5194/gmd-11-3747-2018

Larour, E., Seroussi, H., Morlighem, M., & Rignot, E. (2012). Continental scale, high order, high spatial resolution, ice sheet modeling using the ice sheet system model. *Journal of Geophysical Research*, *117*, F01022. doi: 10.1029/2011JF002140

MacAyeal, D. R. (1989). Large-scale ice flow over a viscous basal sediment: Theory and application to ice stream b, antarctica. *Journal of Geophysical Research: Solid Earth*, *94(B4)*, 4071-4087. doi: 10.1029/JB094iB04p04071

Morland, L. W. (1987). Unconfined ice-shelf flow. In C. J. Van der Veen & J. Oerlemans (Eds.), *Dynamics of the west antarctic ice sheet* (pp. 99–116). Dordrecht: Springer Netherlands. doi: 10.1007/978-94-009-3745-1_6

Morlighem, M. (2020). Measures bedmachine antarctica, version 2. Retrieved from `https://nsidc.org/data/nsidc-0756` (date accessed: 2021) doi: 10.5067/E1QL9HFQ7A8M

Morlighem, M., Rignot, E., Binder, T., Blankenship, D. D., Drews, R., Eagles, G., ... Young, D. A. (2020). Deep glacial troughs and stabilizing ridges un-

veiled beneath the margins of the antarctic ice sheet. *Nature Geoscience*, *13*, 132-137. doi: 10.1038/s41561-019-0510-8

Muszynski, I., & Birchfield, G. E. (1987). A coupled marine ice-stream ice-shelf model. *Journal of Glaciology*, *33*(113), 315. doi: 10.3189/S0022143000005281

Ng, F. S. L., Ignéczi, A., Sole, A. J., & Livingstone, S. J. (2018). Response of surface topography to basal variability along glacial owlines. *Journal of Geophysical Research: Earth Surface*, *123*, 2319-2340. doi: 10.1029/2017JF004555

Pattyn, F. (2017). Sea-level response to melting of antarctic ice shelves on multi-centennial timescales with the fast elementary thermomechanical ice sheet model (f.etish v1.0). *The Cryosphere*, *11*, 1851-1878. doi: 10.5194/tc-11-1851-2017

Pollard, D., & DeConto, R. M. (2012). Description of a hybrid ice sheet-shelf model, and application to antarctica. *Geosci. Model Dev.*, *5*, 1273-1295. doi: 10.5194/gmd-5-1273-2012

Rignot, E., Mouginot, J., Scheuchl, B., van den Broeke, M., van Wessem, M. J., & Morlighem, M. (2019). Four decades of antarctic ice sheet mass balance from 1979–2017. *Proceedings of the National Academy of Sciences*, *116*(4), 1095–1103. doi: 10.1073/pnas.1812883116

Schoof, C. (2006). A variational approach to ice stream flow. *Journal of Fluid Mechanics*, *556*, 227251. doi: 10.1017/S0022112006009591

Schoof, C., & Hewitt, I. (2013). Ice-sheet dynamics. *Annual Review of Fluid Mechanics*, *45*(1), 217-239. doi: 10.1146/annurev-fluid-011212-140632

Shepherd, A., Ivins, E., Rignot, E., & et al. (2018). Mass balance of the antarctic ice sheet from 1992 to 2017. *Nature*, *558*, 219-222. doi: 10.1038/s41586-018-0179-y

Thomas, R. (1973). The creep of ice shelves: Interpretation of observed behaviour. *Journal of Glaciology*, *12*, 55-70. doi: 10.3189/S002214300002270X

Van der Veen, C. (1983). A note on the equilibrium profile of a free floating ice shelf. *IMAU Report V83-15, State University Utrecht*.

Van Wessem, J. M., Reijmer, C. H., Morlighem, M., Mouginot, J., Rignot, E., Medley, B., ... Van Meijgaard, E. (2014). Improved representation of east antarctic surface mass balance in a regional atmospheric climate model. *Journal of Glaciology*, *60*, 761770. doi: 10.3189/2014JoG14J051